https://doi.org/10.5194/essd-2025-822
Preprint. Discussion started: 25 February 2026


Open Access Earth System Science Data Discussions

# Constructing a SWOT Internal Wave Dataset Using Deep Learning

Xinyuan Xi [1,2], Jiahui Chen [1], Ge Chen [1,2], Yuemei Li [1,2], Chunyong Ma [2,1], and Yijie Gai [1]

[1]Department of Marine Technology, Ocean University of China, Qingdao China, 266100
[2]Laoshan Laboratory, Qingdao China, 266237

**Correspondence:** Chunyong Ma (chunyongma@ouc.edu.cn)

**Abstract.** Internal waves (IW) play a crucial role in energy transfer and vertical mixing as key dynamical processes. The Surface Water and Ocean Topography (SWOT) satellite, with its high-resolution sea surface height (SSH) observations, provides new data source for internal wave detecting. This study develops a multi-region automatic internal wave recognition framework named SWOT_IWD and constructs a SWOT internal wave detection dataset (https://doi.org/10.5281/zenodo.17666852, Xi et al. (2025)) covering 13 internal wave-prone regions worldwide from 2023 to 2025. A total of 21,682 SWOT passes are downloaded and processed for internal wave detection across different regions, identifying 2,011 passes containing internal wave signals and detecting a total of 3,264 internal wave signals. The dataset consists of SWOT data and IW labels, and includes visualized internal wave detection result images. The validation results confirm that the average accuracy of the SWOT internal wave dataset is 91.21%. The study analyzes the spatial distribution, activity frequency, and the relationship between internal waves and topographic coupling across 13 regions included in the dataset. We also conducted a quantitative comparison of three data sources: SWOT, Sentinel-1 C-SAR, and Sentinel-3 OLCI. The results indicated that the detection availability of internal waves using SWOT data reached as high as 29.78%. The study demonstrates that this dataset can provide high-quality sample data to support internal wave detection based on deep learning. Furthermore, two cases were presented to illustrate the potential of this dataset for internal wave tracking using multi-source remote sensing data.

## 1 Introduction

Internal waves (IWs), also known as internal solitary waves, are ubiquitous dynamic phenomena. IWs can drive significant vertical mixing and energy flux, with profound implications for oceanic military, engineering, and resource development applications. While the peaks of internal waves can extend over hundreds of kilometers, their wavelengths along the propagation direction range from several hundred meters to a few kilometers, often exhibiting solitary and non-periodic characteristics. These features limit the effectiveness of traditional point-based observations, as well as optical and SAR-based remote sensing, in terms of spatial coverage, temporal continuity, and quantitative capability. The Surface Water and Ocean Topography (SWOT) satellite provides centimeter-level Sea Surface Height (SSH) measurement and wide swath observation. This enables internal wave research to transition from visibility to quantification, allowing for the direct characterization of dynamical signals. Through the spatiotemporal collocation of multi-source observations from SWOT, SAR, and optical sensors, it is possible to further enable three-dimensional reconstruction of internal wave structures and tracking of their propagation pathways,

https://doi.org/10.5194/essd-2025-822
Preprint. Discussion started: 25 February 2026




thereby establishing a new model of cross-sensor synergistic observation (Garrett and Munk (1979); Liu and Hsu (2004); Meng et al. (2024); Ma et al. (2025)).

Traditional approaches to internal wave research have primarily relied on field observations and numerical simulations (Lien et al. (2005)). However, these methods are limited by their restricted spatial coverage, high costs, and low time resolution. To overcome these limitations, satellite remote sensing has emerged as a promising solution for large-scale, high-precision detection of internal waves. Mainstream optical remote sensing satellites, such as MODIS and VIIRS, are constrained by weather conditions and diurnal variations (Jackson (2007); Liu and D'Sa (2019)), while SAR like ENVISAT and Sentinel-1 face challenges due to insufficient coverage(Ma et al. (2022); Liu et al. (2014)). In contrast, the SWOT satellite, with its centimeter-level Sea Surface Height (SSH) measurements and wide-swath observations, overcomes the limitations of optical data and SAR data (Zhang and Li (2024a); Liu and D'Sa (2019)). As remote sensing techniques evolve, new challenges are emerging for methods of detecting internal waves. Early internal wave detection primarily relied on manual interpretation, which was insufficient for handling large-scale data processing. As a result, the focus of research has gradually shifted towards efficient and automated detection methods (Rodenas and Garello (1997); Kang et al. (2008); Arvelyna (2010); Simonin et al. (2009); Cui et al. (2025)). Recently, machine learning algorithms have shown significant progress in enhancing the accuracy of internal wave detection (Geng et al. (2016); Gan et al. (2007, 2008)). However, these methods often rely on manually designed features, which limits their performance and generalization, particularly in complex marine environments. With the advancement of object detection and deep learning, these techniques have been increasingly applied to ocean remote sensing, achieving remarkable results (Duo et al. (2019); Li et al. (2020)). Methods such as the PCANet framework (Dong et al., 2018) and the modified U-Net network (Vasavi et al. (2021)) have been successfully utilized in internal wave detection.

The development of these methods has not only significantly enhanced the automatic detection capability of internal waves but also directly facilitated the construction and development of large-scale, standardized internal wave datasets. Santos-Ferreira et al. (Santos-Ferreira et al. (2022)) proposed the first global automatic internal wave detection system, the Internal Waves Service (IWS), at the International Internal Waves Symposium (IWS-W25). Based on Sentinel-1 SAR imagery and deep learning algorithms, they developed an internal wave event dataset covering the open ocean and hotspot regions, such as the South China Sea and the Equatorial Pacific. However, internal wave labels were not provided. Ma et al. (Ma et al. (2024)) constructed the first deep learning dataset for internal wave detection, S1-IW-2023, which also relies on SAR imagery and provides all-weather observation capabilities. However, the samples are mostly concentrated in hotspot regions like the Andaman Sea and South China Sea, with sparse coverage in other areas. Furthermore, due to the limitations of SAR imaging modes and WV coverage, ensuring the spatiotemporal continuity of internal wave observations remains challenging. On the other hand, Zhang and Li (Zhang and Li (2024b)) focused on the northern South China Sea, using MODIS data from 2000 to 2022 and the IWE-Net model to construct an internal wave dataset with a spatial resolution of 250 meters. Although current research has advanced the development of internal wave datasets from three perspectives: global detection systems, specialized datasets, and long-term regional analysis, there are still limitations. First, there is uneven geographic coverage. While IWS and S1-IW-2023 provide global coverage, SAR data is insufficient in open ocean regions, and the sample distribution is highly concentrated in hotspot areas. Although the dataset by Zhang and Li offers a long time series, it is limited to the northern South China Sea and

https://doi.org/10.5194/essd-2025-822
Preprint. Discussion started: 25 February 2026


Open Access Earth System Science Data Discussions

lacks global representativeness. Second, existing internal wave datasets rely on single data sources. SAR data is constrained by revisit cycles and imaging mechanisms, while optical data is susceptible to cloud cover and weather interference. Both factors lead to observational gaps and hinder continuous monitoring.

In the context of significant advancements in both internal wave remote sensing techniques and detection algorithms, the global high-resolution Sea Surface Height (SSH) data provided by the SWOT satellite offers new opportunities for constructing next-generation internal wave datasets. The SWOT satellite is equipped with the Ka-band Interferometric Radar (KaRIN), which offers advantages such as all-weather capability, high precision, and wide swath coverage, providing revolutionary observational conditions for oceanic internal wave research (Zhang et al. (2024)). SWOT can obtain global high-resolution SSH data, addressing the limitations of traditional observations in spatial coverage and time resolution, and providing unprecedented potential for exploring the spatiotemporal distribution and dynamics of large-scale internal waves (Qiu et al. (2024)). Compared to optical and SAR data, which are susceptible to external factors such as wind fields, oil films, waves, and cloud cover, SWOT data can directly visualize the two-dimensional SSH field, enabling the study of internal wave energy and phase structures (Zhang et al. (2024); Fu et al. (2024); Wang et al. (2025)). Furthermore, SWOT can be integrated with multi-source data, such as optical and SAR, to enable continuous internal wave tracking, thereby enhancing the physical consistency and robustness of multi-source fusion (Pan et al. (2025); Cai et al. (2024); Fu et al. (2024); Da Silva et al. (2025)). However, research on internal waves using SWOT data is still in its early stages. There is a gap in the development of universal internal wave detection models for key marine areas, and a systematic internal wave dataset based on the next-generation altimeter has yet to be established. Building an internal wave dataset based on SWOT not only fills the existing research gap but also lays the foundation for automated detection, process analysis, and predictive modeling.

Therefore, the aim of this study is to develop a multi-region internal wave detection model based on SWOT data, designed to automatically extract internal wave features from SWOT data. A comprehensive, accessible, and high-quality large-scale internal wave deep learning dataset has been established, providing valuable resources for deep learning-based internal wave sample support and dynamic monitoring. The paper is organized as follows: Section 2 describes the satellite data and deep learning models; Section 3 presents the detection results and multi-source validation; Section 4 highlights the dataset statistics, applications, and findings from the SWOT internal wave dataset; Section 5 discusses data acquisition; Section 6 provides conclusions and future perspectives.

## 2 Data and methods

### 2.1 SWOT Data

The SWOT satellite is a major international Earth observation mission jointly led by the National Aeronautics and Space Administration (NASA) and the French Centre National Études Spatiales (CNES). It was launched on 16 December 2022. The satellite is designed to achieve high-accuracy, high spatial-resolution topographic measurements of global surface water and oceanic water bodies, marking the advent of a new era of wide-swath, two-dimensional elevation remote sensing for the oceans. SWOT operates in a near-polar, sun-synchronous orbit with an altitude of approximately 891 km, an inclination of 77.6°, and a

https://doi.org/10.5194/essd-2025-822
Preprint. Discussion started: 25 February 2026


Open Access Earth System Science Data Discussions

21-day repeat cycle. Its primary payload is the Ka-band Radar Interferometer (KaRIN), which adopts a dual-antenna interferometric configuration with a 10 m baseline and a central frequency of 35.75 GHz. KaRIN provides a swath width of about 120 km, enabling high-resolution two-dimensional measurements of sea surface height. Figure1. shows the global ground-track coverage of SWOT. In this study, we use the SWOT Level-2 Sea Surface Height Anomaly (SSHA) product, which effectively highlights sea surface undulation signals induced by internal waves. The SSHA data are processed and distributed by AVISO and other internationally recognized ocean data centers, providing an unprecedented global, high-resolution observational basis for the detection and investigation of internal waves. Using SWOT data from 30 March 2023 to 14 September 2025, we construct an internal-wave dataset, comprising a total of 21,682 SWOT ground tracks. The number of SWOT overpasses in each study region is summarized in Table 1.

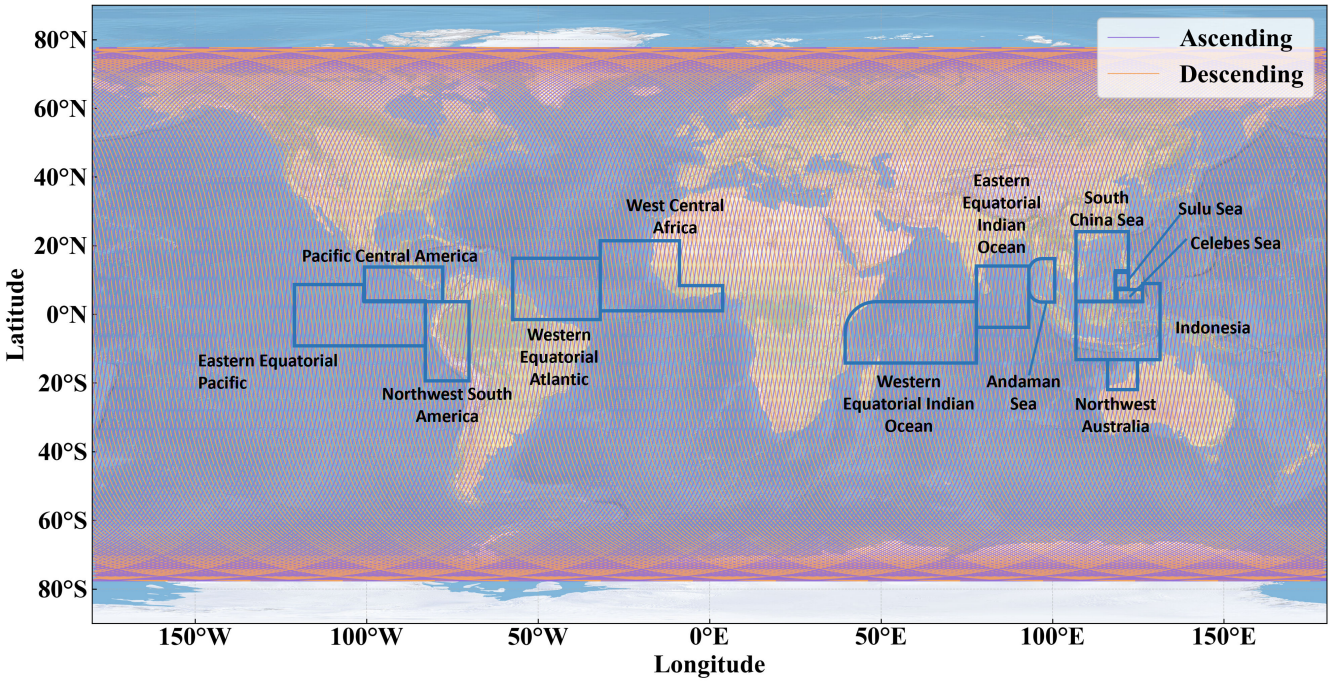


**Figure 1.** SWOT Orbit Coverage and Distribution Map of Internal Wave-Prone Regions.

Based on optical remote sensing observations of internal waves, this study selects 13 regions with frequent internal wave activity, distinct spatial distribution characteristics, and well-defined dynamical backgrounds as the study areas. According to MODIS observation statistics, the number of internal wave occurrences varies markedly among global oceans. The Indonesia region has 465 detected internal wave events, making it the most active internal wave region globally. This is followed by the Western Equatorial Indian Ocean with 324 events and the South China Sea with 278 events. Other regions include Pacific Central America with 234 events, the Andaman Sea with 231 events, West Central Africa with 192 events, the Western Equatorial Atlantic with 180 events, the Sulu Sea with 142 events, and the Eastern Equatorial Indian Ocean with 123 events. In addition, 112 internal wave events are observed off Northwest Australia, 104 in the Eastern Equatorial Pacific, 83 off Northwest South

https://doi.org/10.5194/essd-2025-822
Preprint. Discussion started: 25 February 2026




**Table 1.** Number of SWOT Satellite Passes Over Frequent Internal Wave Regions

| | **SWOT Data Volume Over the Region /Pass** |
|---|---|
| Eastern Equatorial Pacific | 3273 |
| Western Equatorial Indian | 2381 |
| Indonesia | 1523 |
| Western Equatorial Atlantic | 1417 |
| South China Sea | 1207 |
| Eastern Equatorial Indian | 1163 |
| West Central Africa | 1137 |
| Northwest South America | 798 |
| Pacific Central America | 782 |
| Northwest Australia | 753 |
| Andaman Sea | 694 |
| Celebes Sea | 659 |
| Sulu Sea | 561 |

America, and 69 in the Celebes Sea Jackson (2007). The selected regions are not only characterized by high occurrence frequency and broad geographical coverage, but most of them also exhibit a clear tide–topography generation mechanism and good detectability in remote sensing imagery. They are therefore well suited for investigating the generation mechanisms and propagation characteristics of internal waves, as well as their interactions with the marine environment. Based on the activity level, geographical representativeness, and dynamical typicality of internal waves in these regions, this study takes these areas as key targets for analysis, with the aim of systematically exploring the spatiotemporal distribution patterns of internal waves and constructing an internal wave dataset for major global hotspots. Figure2. presents SWOT observations over the Western Equatorial Indian Ocean and the Western Equatorial Atlantic, illustrating that SWOT provides near-complete coverage and clearly identifiable internal wave signatures over these two broad oceanic regions.

## 2.2 Remote Sensing Collaborative Verification Data

This study integrates multi-source remote sensing data to verify that the internal wave signals detected by SWOT are genuine, Regarding data sources, we first employ synthetic aperture radar (SAR) data from Sentinel-1. Sentinel-1 is a key satellite mission within the Copernicus Programme led by the European Space Agency (ESA), equipped with a C-band Synthetic Aperture Radar (C-SAR) sensor that provides all-weather, day-and-night imaging capabilities. One of its main products is the Level-1 Ground Range Detected (GRD) dataset, a pre-processed SAR image product. GRD data are intensity images generated after multi-looking, slant-range to ground-range projection, and radiometric and geometric corrections. The GRD products provide single- or dual-polarization amplitude images without phase information, making them highly suitable for

https://doi.org/10.5194/essd-2025-822
Preprint. Discussion started: 25 February 2026


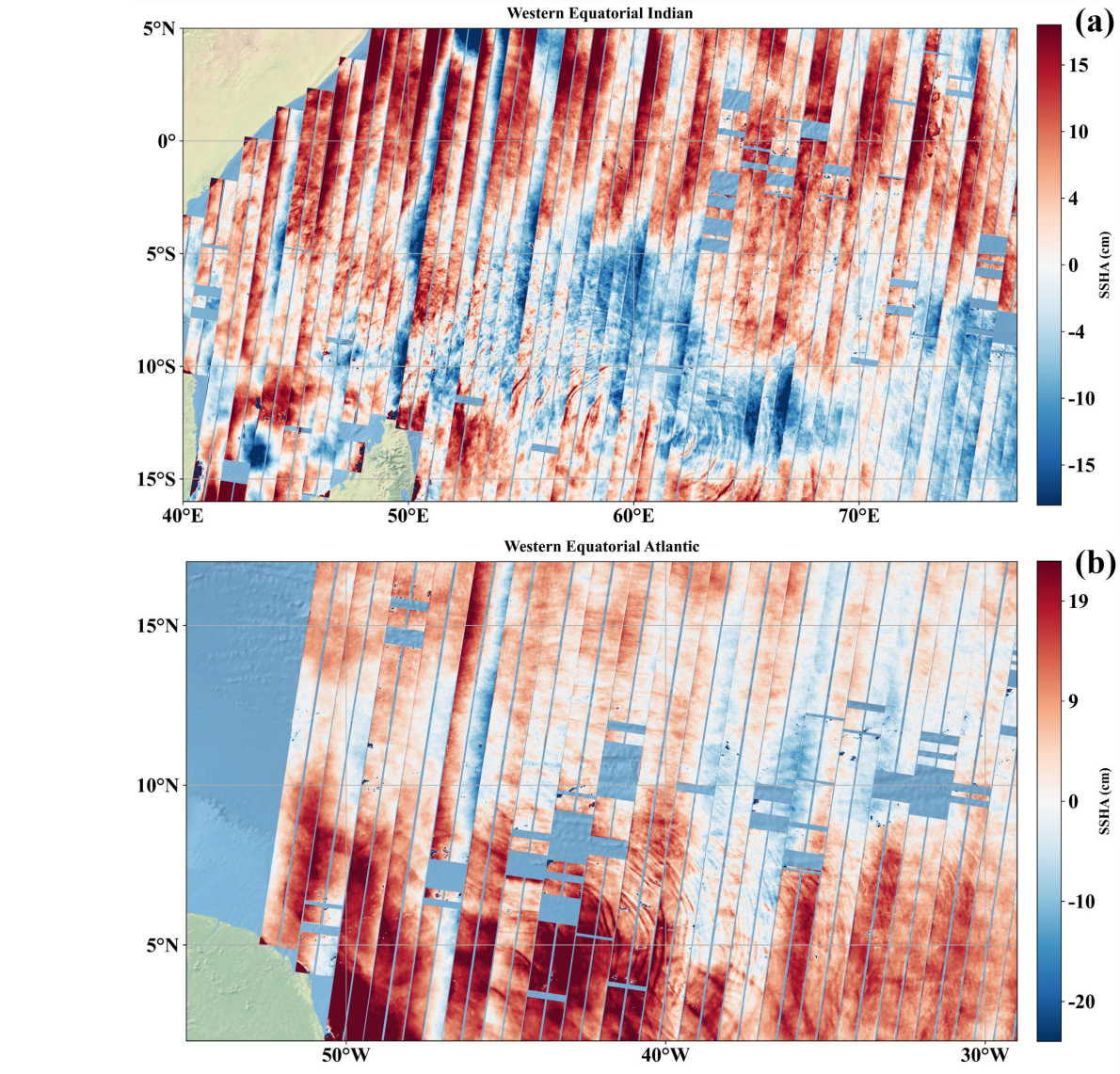


**Figure 2.** Example SWOT Satellite Pass Coverage Over the Study Regions(a) Western Equatorial Indian, (b) Western Equatorial Atlantic.

surface target monitoring and image interpretation. These data feature a relatively wide swath; in Interferometric Wide (IW) mode, a single acquisition can cover an area of up to 250 km, enabling large-scale monitoring. In addition, supported by the two-satellite constellation, Sentinel-1 can achieve high-frequency repeat coverage with a revisit interval of no more than six days(Svergun et al. (2023); Meng et al. (2022); Cao et al. (2024)).

In addition to SAR data, this study also employs optical remote sensing data provided by Sentinel-3 to validate the SWOT internal wave observations. The Ocean and Land Colour Instrument (OLCI) onboard Sentinel-3 is one of its primary sensors.

https://doi.org/10.5194/essd-2025-822
Preprint. Discussion started: 25 February 2026




OLCI is an optical imaging instrument with 21 spectral bands, covering wavelengths from the visible to the near-infrared (400–1020 nm), with a wide swath of 1,270 km and a spatial resolution of 300 m. The orbital configuration of Sentinel-3 enables high-frequency global revisits every 2–3 days, providing strong support for the continuous monitoring of dynamic environmental processes (Yu et al. (2023); Santos-Ferreira et al. (2022)). By using Sentinel-3 OLCI data, the reliability of the internal wave dataset can be effectively assessed, thereby supporting the validation of the accuracy of SWOT internal wave detections.

### 2.3 Deep learning model

To enable the intelligent detection of internal waves from SWOT data, this study introduces the SWOT_IWD model, specifically designed for SWOT altimeter data. The model is built upon the YOLOv11 architecture, leveraging its efficiency and real-time detection capabilities (Yang et al. (2025); Lee and Kim (2024)). The model performs multi-dimensional optimization based on the morphology and texture of internal waves in SSHA data, aiming to reliably detect the elongated internal wave signal within complex sea surface height data. Considering the multi-scale, low-contrast, and high-background characteristics of internal wave signals in SWOT data, an Adaptive Feature Enhancement (AFE) module is introduced into the network. This module adaptively extracts and amplifies the input features, further enhancing the model's overall representation capability.

In the SWOT L2 SSHA data, the background occupies a significant proportion of the data, while internal wave targets appear as elongated, low-contrast streaks, resulting in a highly imbalanced sample distribution. Traditional Focal Loss uses a fixed focusing factor to suppress the gradients of easily detectable samples. However, its assumption of fixed discrimination threshold is not well-suited for adapting to the spatial and temporal variability of internal wave textures. To balance high recall and low false detection rates, this study introduces Adaptive Threshold Focal Loss (ATFL) as the core loss function for the classification branch. The goal is to enhance the weighting mechanism for different samples by adaptively adjusting the modulation factor $\gamma$ in the loss function. ATFL specifically focuses on hard-to-classify samples and dynamically adjusts the threshold $\gamma$ to accommodate the characteristics of different samples, thereby addressing the class imbalance issue more effectively. The value of $\gamma$ is dynamically adjusted based on the average predicted probability pt, enabling the model to adaptively weight samples based on their difficulty. The ATFL loss function incorporates different weighting schemes for $p_t$>0.5 and $p_t \leq 0.5$, and adjusts the weights using $\gamma$, making the loss function more flexible. The ATFL loss function calculates the standard binary cross-entropy loss and dynamically adjusts the weighting factor based on the predicted probability pt. The specific formula is as follows:

$$L_{\text{ATFL}} = -\alpha_t \cdot (1 - p_t)^{\gamma_t} \log(p_t) \tag{1}$$

In this formulation, $\alpha_t$ is a balancing factor that adjusts the weighting between positive and negative samples; $p_t$ is the predicted probability (where $p_t = \sigma(\hat{y})$, and $\sigma(\hat{y})$ is the output of the model after Sigmoid activation); $\gamma_t$ is an adaptive tuning factor that depends on the current sample's predicted probability $p_t$, and $\log(p_t)$ represents the standard logarithmic loss used to compute the cross-entropy for the class. The key innovation of ATFL lies in its adaptive adjustment of $\gamma$. Specifically, $\gamma_t$ varies dynamically based on the sample's predicted probability $p_t$, and the average predicted probability of such samples. The

https://doi.org/10.5194/essd-2025-822
Preprint. Discussion started: 25 February 2026


ATFL is calculated as follows:

$$\gamma_t = -\log\left(\frac{1}{100} + \alpha \cdot p_t\right) \tag{2}$$

Here,$\alpha$ is a tuning factor, typically set to 0.05. This adjustment method enables ATFL to apply smaller weighting factors to easily classified samples, while applying larger weighting factors to more difficult-to-classify samples, thereby placing greater emphasis on the training of challenging samples. This adaptive adjustment mechanism helps the model focus better on hard-to-classify samples, especially in cases of class imbalance or when foreground targets are scarce, thereby improving the detection accuracy of the model. ATFL offers greater flexibility and precision, enabling the model to smoothly handle samples of varying difficulty levels. It automatically adjusts the weighting factors when facing different sample prediction probabilities, preventing background samples from dominating the loss. Therefore, ATFL is particularly suited for handling highly imbalanced datasets. In target detection tasks, especially for small or densely packed targets, ATFL significantly improves the model's robustness and accuracy, ensuring that foreground targets receive sufficient training attention, thereby effectively enhancing target detection performance.

At the structural and representational level, SWOT_IWD enhances sensitivity to internal waves of varying wavelengths by employing a more efficient backbone network and multi-scale feature fusion. Additionally, dynamic label assignment is used to improve the coverage of positive samples, particularly for elongated, low-contrast targets. The model introduces the AFE module as a key feature enhancement unit, which consists of two parallel components: the Spatial Context Module (SCM) and the Feature Refinement Module (FRM). The SCM expands the receptive field and aggregates global context to model the relationship between the target and background, while the FRM focuses on local edges and textures to refine the expression of details. The combination of these two modules enables adaptive enhancement for internal wave detection, effectively suppressing background interference while emphasizing the morphological details of internal wave streaks. This approach is particularly well-suited for object detection tasks that rely on both global context and local details. In summary, the adoption of ATFL enables adaptive weighting of imbalanced samples, while AFE provides adaptive context and detail enhancement at the feature level. Together with the decoupled detection head and multi-channel input with physical priors, these components form a closed-loop synergy. On one hand, ATFL suppresses the competitive influence of high-confidence negative samples during matching, reducing false detection rates. On the other hand, it enhances separability under multi-scale and complex backgrounds, maintaining a high recall rate. This systematic approach effectively alleviates the challenges of internal wave remote sensing detection. The model framework is shown in Figure3.

### 2.4 Post-processing

The internal wave dataset constructed by SWOT_IWD in this study achieved an average accuracy of 91.21%, with approximately 8.79% of model classifications being false positives. These inaccuracies are primarily caused by a small subset of features resembling internal wave (IWS), such as noise generated at the land-sea boundary, near coastal areas, or around small islands, as well as minor surface fluctuations caused by shallow water topography. These small-scale misclassifications are stored in pixel coordinate label format, allowing users to perform additional post-processing as needed.

https://doi.org/10.5194/essd-2025-822
Preprint. Discussion started: 25 February 2026


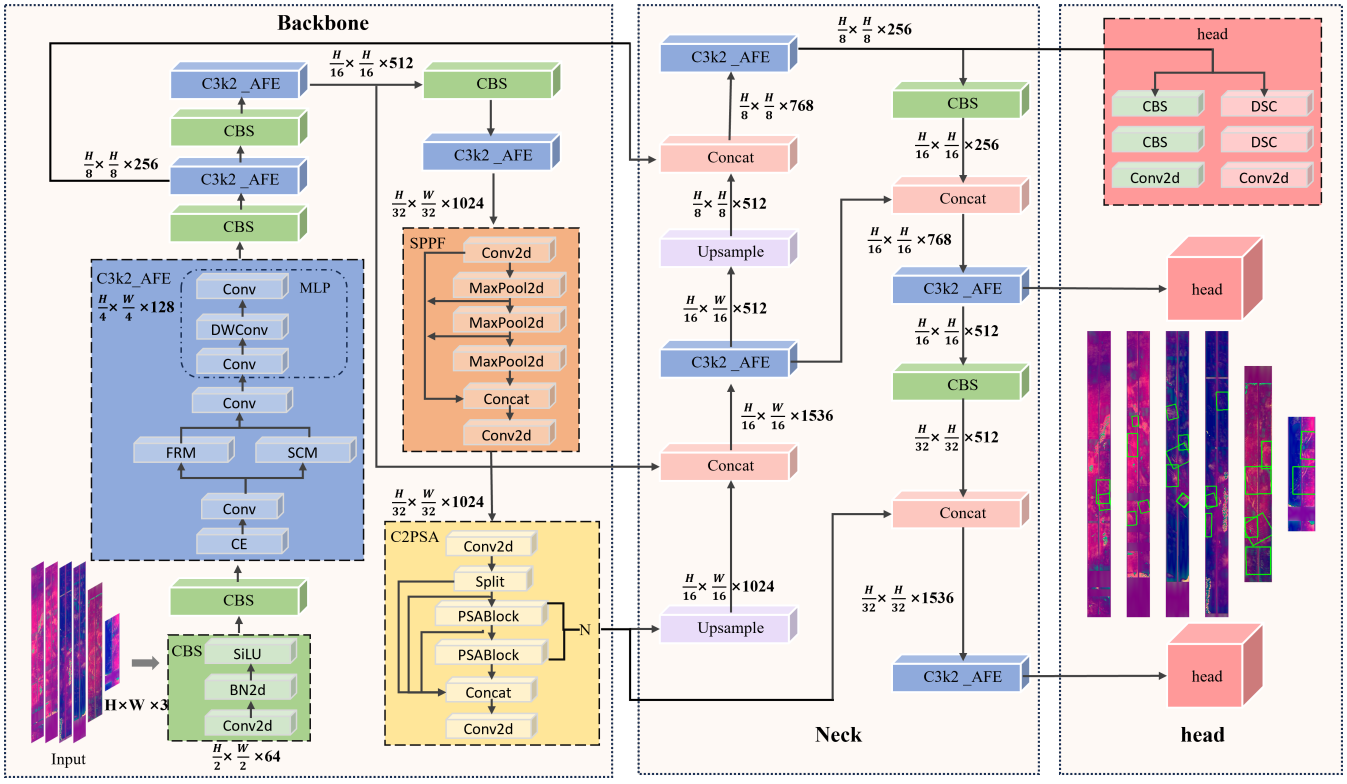


**Figure 3.** The framework of the proposed SWOT_IWD.

## 2.5 Data records

This study generated two sets of data: regional SWOT data with observed IW labels and corresponding IW location information. All data have been archived and stored in the database at https://doi.org/10.5281/zenodo.17666852 (Xi et al. (2025)).

### 2.5.1 SWOT IW imagery

The source data for internal wave observations in this study were derived from the SWOT L2 LR SSH Expert Product (NetCDF-4.nc). The SWOT data for each study region are stored in local directories corresponding to the respective regions. The file naming structure and its meaning are as follows:

SWOT_L2_LR_SSH_<FileIdentifier>_<CycleID>_<PassID>_<RangeBeginningDateTime>_<RangeEndingDateTime>_<CRID>_<ProductCounter>.nc

1) **FileIdentifier:** Represents the file category, including Basic, WindWave, Expert, and Unsmoothed.
2) **CycleID:** Denotes the repeat cycle number.
3) **PassID:** Identifies the orbit number.

https://doi.org/10.5194/essd-2025-822
Preprint. Discussion started: 25 February 2026


4) **RangeBeginningDateTime, RangeEndingDateTime:** Represents the UTC time range covered by the data used to generate the product, formatted as YYYYMMDDThhmmss.

5) **CRID:** Composite Release Identifier, which includes the version code of the product. This code changes when processing software and/or auxiliary inputs are updated.

6) **ProductCounter:** When the same product is generated multiple times under the same processing version, this counter is used to distinguish between different versions of the generated product.

To highlight the texture of internal wave streaks, this study enhances SWOT data by applying Fourier Transform (FFT) and Discrete Wavelet Transform (DWT). FFT transforms the image from the spatial domain to the frequency domain, separating low and high frequencies to facilitate frequency-domain denoising and edge enhancement. DWT possesses multi-scale and spatiotemporal localization properties, making it more effective in capturing edges and details in non-stationary signals. The combination of both processing methods helps suppress non-internal wave data while enhancing the contrast and clarity of internal wave patterns. The three-channel composite TIF is used solely for the visualization and quality checking of internal wave detection results and is not included as part of the image layer in the dataset. The sole basis for the image layer in the dataset remains the SWOT L2 LR SSH Expert.nc. The overlay images are intended to present the visual features of the sea surface height data, enhanced through frequency-domain and multi-scale techniques, more clearly, to aid in internal wave identification and manual verification.

### 2.5.2 IW overlay imagery

The internal wave detection labels are in the format of Oriented Bounding Boxes (OBB). Each SWOT dataset undergoes full-image or sliding window detection, with the results overlaid as vector boxes on the visualized images. The output labels and center point coordinates are normalized. The directory and format are as follows:

1) **data/:** Contains SWOT data with internal wave signals.

2) **images/:** Visualized data with detection boxes drawn.

3) **labels/:** TXT label files, named the same as the SWOT data, in the YOLO-OBB normalized format. These labels use a 4-vertex polygon format with 8 values, where the coordinates are in pixel format. class_id represents the class identifier, with internal waves labeled as 0 in this study.

4) **centers/:** The center positions of each internal wave detection target (saved as *_centers.txt).

## 3 IW signature extraction and validation

This study developed the SWOT_IWD model for detecting internal wave signals in SWOT data. To assess the applicability of the model, detection was performed over 13 global regions with frequent internal wave activity. The SWOT data used covers the period from March 30, 2023, to September 14, 2025, encompassing internal wave activity across multiple seasons and diverse

https://doi.org/10.5194/essd-2025-822
Preprint. Discussion started: 25 February 2026


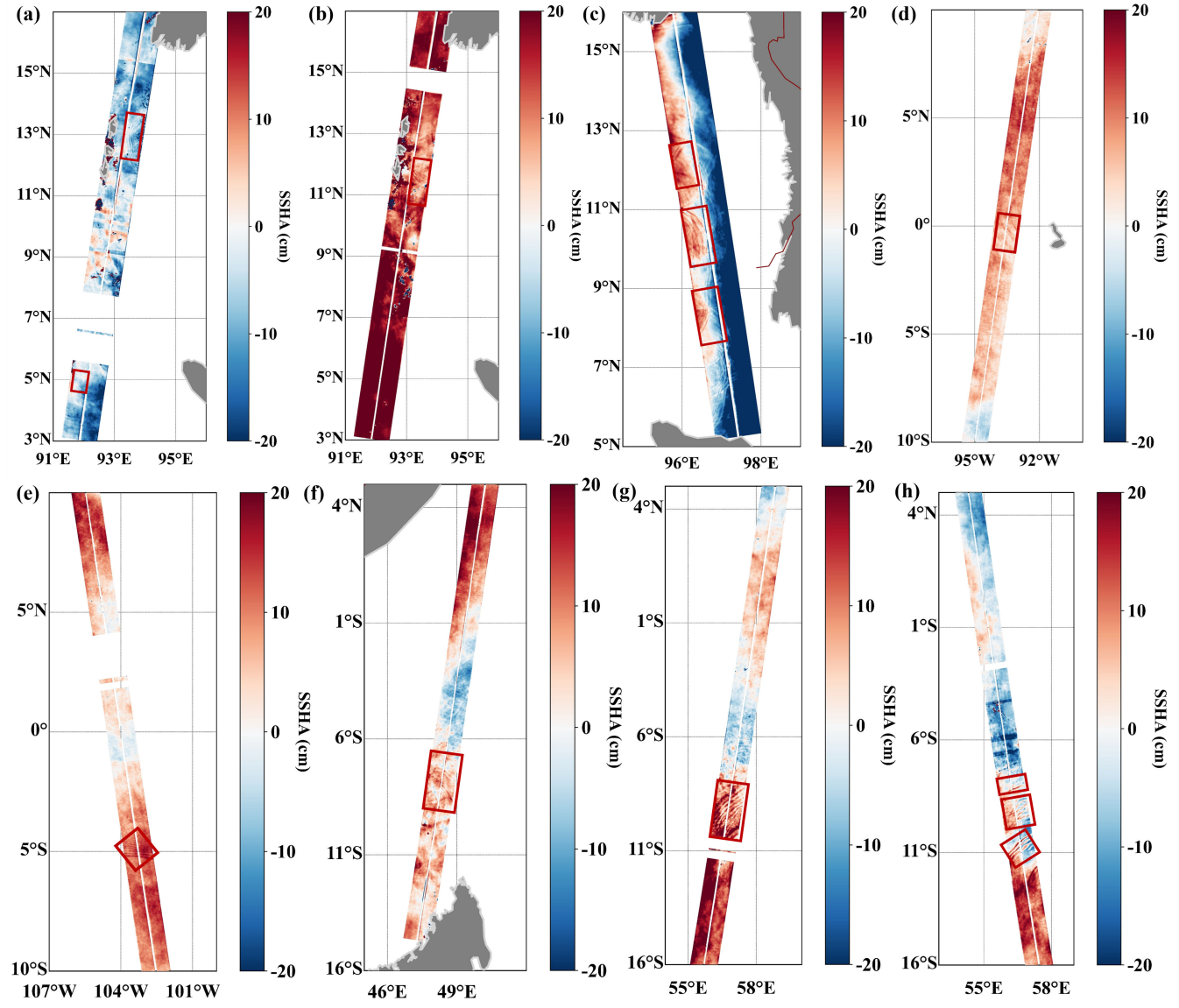


**Figure 4.** SWOT Data and Internal Wave Label Example Figure. (a)-(h) show detection results from different regions, with the red box indicating the detection box location.

245 To further evaluate the accuracy of the model detection results, this study performs a comparative analysis using multiple remote sensing datasets. Figure5 presents the validation results comparing SWOT data with Sentinel-3 OLCI optical data,

https://doi.org/10.5194/essd-2025-822
Preprint. Discussion started: 25 February 2026




where the complementary nature of their observation principles provides strong support for the verification process. Figure6 displays the comparison between SWOT data and Sentinel-1 C-SAR data. Using synthetic aperture radar technology, Sentinel-1 C-SAR data allows efficient detection even under cloud cover and adverse weather conditions, thus enhancing the reliability of the validation results. Figure7 shows the cross-validation results among SWOT data, Sentinel-3 OLCI optical data, and Sentinel-1 C-SAR data. The three datasets, based on different physical principles, complement each other and strengthen the credibility of the detection results from the perspectives of SSH, backscatter coefficients, and spectral radiance. These comprehensive validation approaches effectively demonstrate the authenticity, reliability, and practical applicability of the model detection results.

The following presents several examples of internal wave detection using SWOT data. Figure5(a) shows an internal wave (IW) detected by SWOT on January 2, 2024, at 07:50, compared with the optical image from Sentinel-3 OLCI on January 1, 2024, at 02:15 and 02:18 (Figure5(b)), with the corresponding IW region highlighted in a red box. Figure6(a) shows an IW detected by SWOT on January 13, 2024, at 06:13, while Figure6(b) presents the corresponding SAR image from Sentinel-1 C-SAR, acquired on January 12, 2024, at 21:49, marking the IW region. Lastly, Figure7(a) shows another IW detected by SWOT on March 25, 2024, at 03:09, and compares it with the SAR image from Sentinel-1 C-SAR on March 12, 2024, at 21:49 (Figure 7(b)), as well as the optical image from Sentinel-3 OLCI on March 26, 2024, at 02:15 (Figure 7(c)). In all these images, the red boxes clearly highlight the IW regions, demonstrating the effectiveness of combining SWOT with other satellite data for internal wave observation.

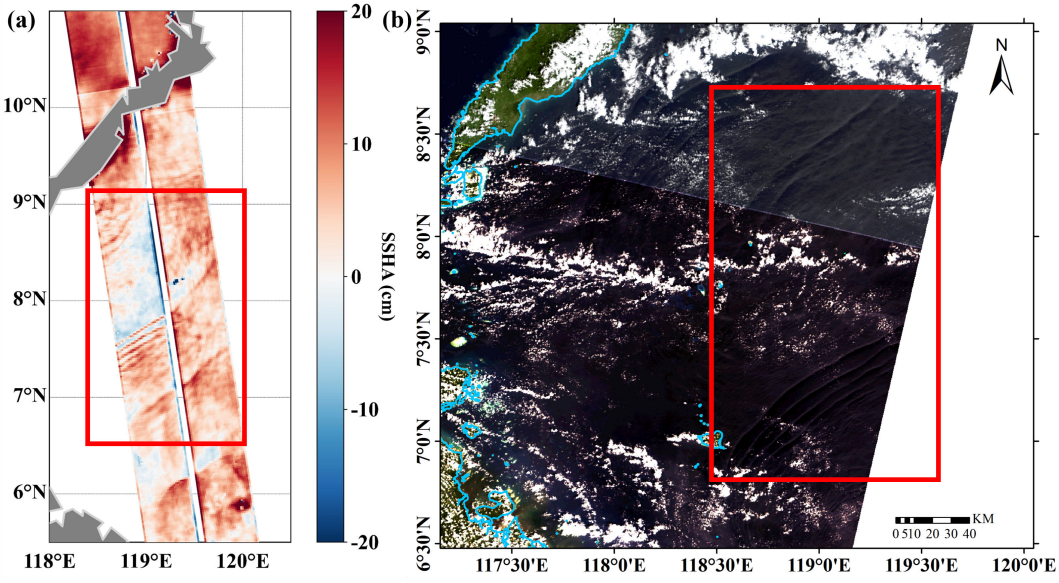


**Figure 5.** Example of an internal wave (IW) detected by SWOT on 02 January 2024 at 07:50 UTC. (a) corresponds to the SWOT data, while (b) shows the optical image (from Sentinel-3 OLCI, 01 January 2024 at 02:15 and 02:18 UTC). The red boxes indicate the corresponding areas where the IW appears.

https://doi.org/10.5194/essd-2025-822
Preprint. Discussion started: 25 February 2026


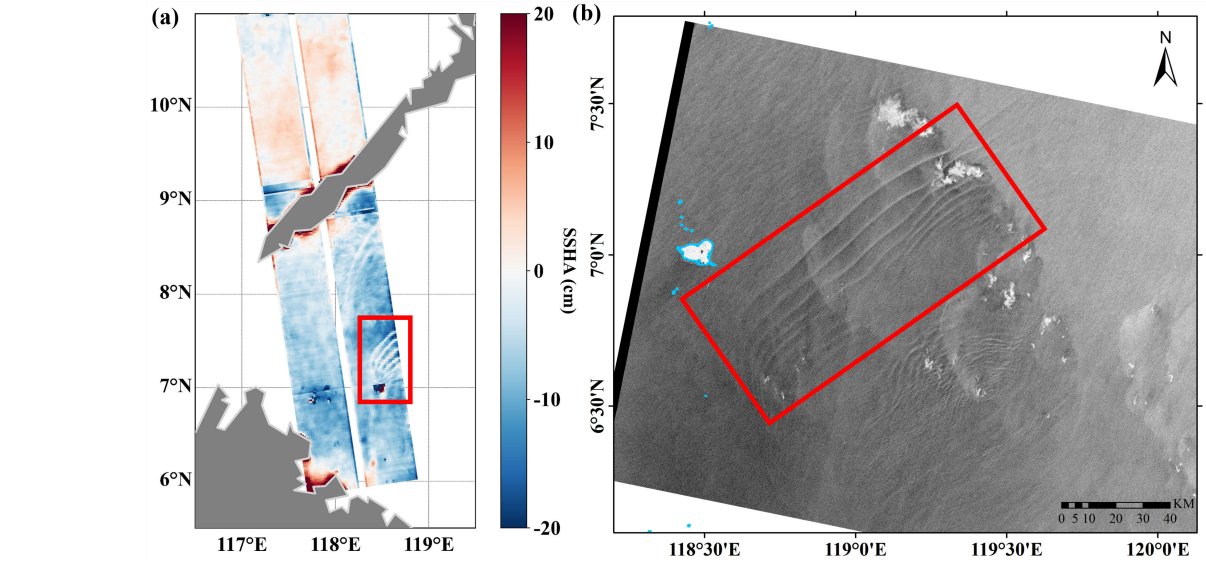


**Figure 6.** Example of an internal wave (IW) detected by SWOT on 13 January 2024 at 06:13 UTC. (a) corresponds to the SWOT data, while (b) shows the SAR image (from Sentinel-1 C-SAR, 12 January 2024 at 21:49 UTC). The red boxes indicate the corresponding areas where the IW appears.

## 4 Statistical analysis

### 4.1 SWOT IW spatial distributions

This study used SWOT data from 2023 to 2025 to detect internal waves in 13 global regions. Figure8 visualizes the central points of internal wave signal locations in each region to illustrate the spatial distribution of internal wave signals observed by SWOT across different marine areas.

The internal wave detection results from the SWOT satellite in the Andaman Sea region indicate that SWOT successfully detected internal waves, primarily distributed between 5°N and 13°N, covering most of the Andaman Sea. The generation of internal waves in the Andaman Sea is closely related to the complex interactions between tidal currents and seafloor topography. When tidal currents pass over underwater features such as Car Nicobar and Batti Malv islands, strong tidal forces cause vertical density variations in the seawater, which in turn trigger the formation of internal waves. In specific areas of the Andaman Sea, the generation of internal waves is intensified by nonlinear amplification of internal tides. When tidal currents interact with underwater ridges, the originally linear internal tidal waves become steeper and eventually evolve into internal wave packets. Internal waves in the Andaman Sea primarily originate from the strait between Car Nicobar and Teresa Island. The internal waves propagate eastward into the Andaman Sea and westward into the Bay of Bengal. Along the seabed's slope and depth variations, the speed and waveform of the internal waves change. During propagation, the internal waves may split into multiple packets and gradually dissipate when they reach shallower regions. This is due to the influence of the seafloor topography,

https://doi.org/10.5194/essd-2025-822
Preprint. Discussion started: 25 February 2026


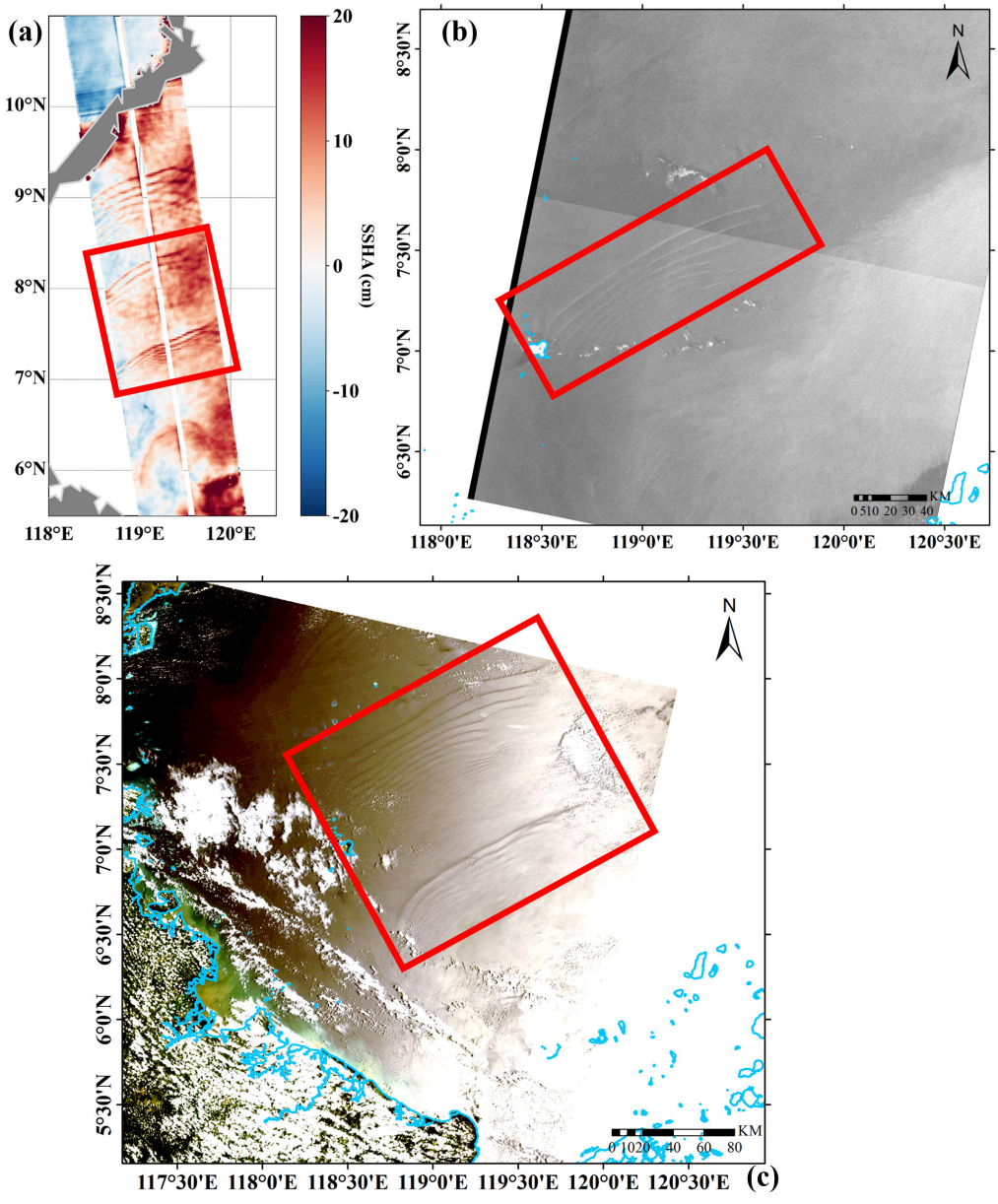


**Figure 7.** Example of an internal wave (IW) detected by SWOT on 25 March 2024 at 03:09 UTC. (a) corresponds to the SWOT data, (b) shows the SAR image (from Sentinel-1 C-SAR, 12 March 2024 at 21:49 UTC), and (c) displays the optical image (from Sentinel-3 OLCI, 26 March 2024 at 02:15 UTC). The red boxes indicate the corresponding areas where the IW appears.

280 especially when internal waves approach underwater ridges or shallow areas, where the wave intensity weakens and eventually disappears. This propagation pattern allows internal wave signals to be monitored by the SWOT satellite over extended time

https://doi.org/10.5194/essd-2025-822
Preprint. Discussion started: 25 February 2026


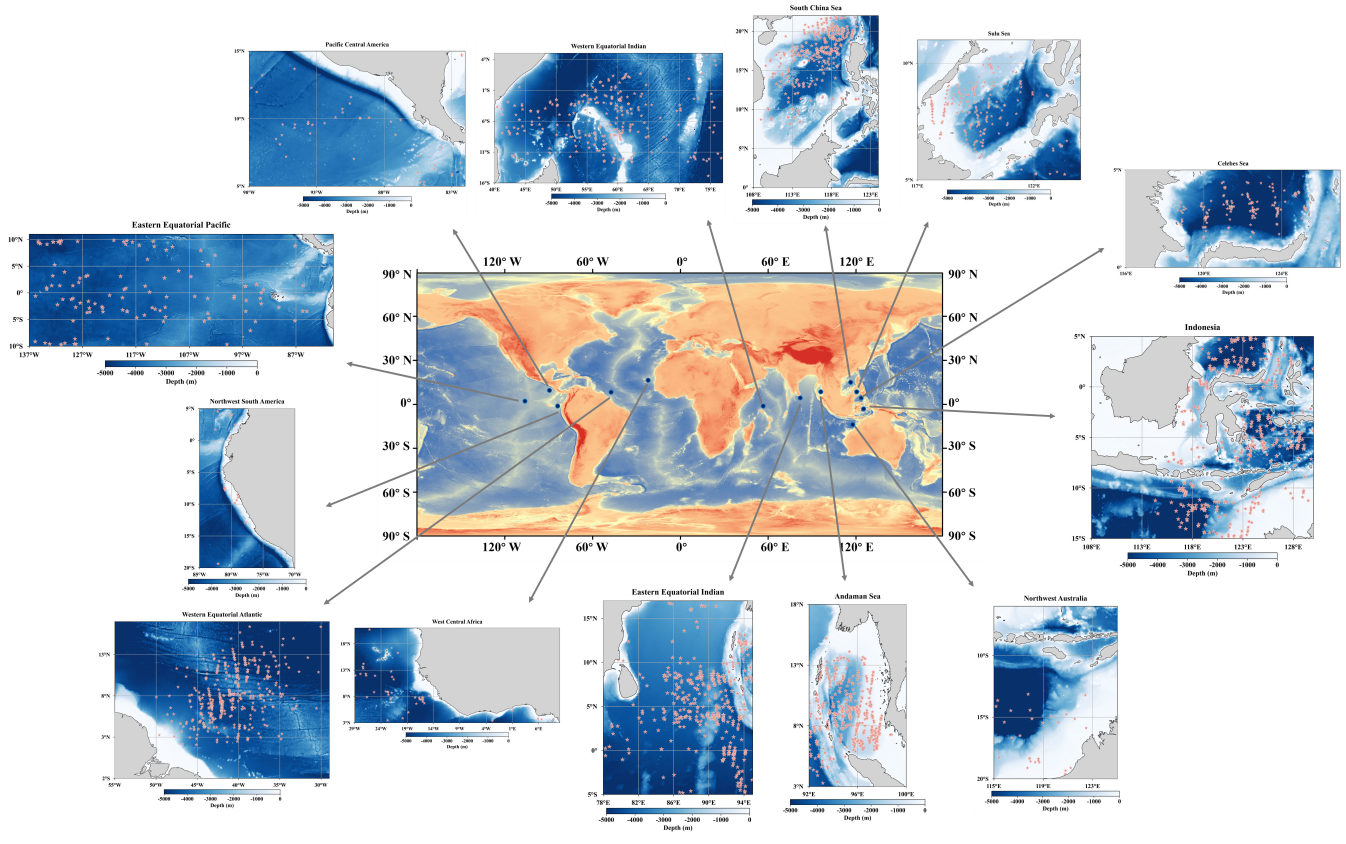


**Figure 8.** Spatial Distribution Map of the SWOT Internal Wave Dataset.

scales, with a relatively stable distribution pattern. The distribution of internal wave signals in the Andaman Sea is dense, especially near deeper areas of the seafloor. This suggests that SWOT can effectively cover this region and capture internal wave signals associated with changes in seafloor topography(Mandal et al. (2024); Sun et al. (2024); Yu et al. (2023)).

The internal wave detection results from the SWOT satellite in the South China Sea region show that SWOT internal wave observations are mainly concentrated between 15°N and 20°N, covering a wide distribution area. Notably, the internal wave signals are more densely distributed in the northern and western regions. The generation of internal waves in the South China Sea is primarily driven by the interaction between tidal currents and complex seafloor topography, the influence of monsoons and hydrological conditions, as well as local generation mechanisms. When tidal currents pass through regions with significant topographic changes such as deep-sea basins, straits, and seafloor ridges, vertical density structure changes in the water lead to the generation of internal waves. The monsoons enhance the surface water temperature gradient and promote vertical stratification of seawater, providing a favorable environment for internal wave formation. Additionally, some internal waves may also be generated locally through the interaction of tides and subtidal flows and the influence of seafloor undulations, particularly in the seafloor slopes and shallow water regions. Overall, the generation mechanisms of internal waves in the South China Sea exhibit

https://doi.org/10.5194/essd-2025-822
Preprint. Discussion started: 25 February 2026




**Table 2.** Statistics of SWOT passes with detected internal waves and the number of detected internal waves in the dataset.

| | Number of SWOT passes with detected internal waves/Pass | Number of detected internal waves |
|---|---|---|
| Andaman Sea | 198 | 580 |
| Indonesia | 280 | 476 |
| Eastern Equatorial Indian | 238 | 446 |
| Western Equatorial Atlantic | 279 | 429 |
| South China Sea | 252 | 363 |
| Western Equatorial Indian | 217 | 269 |
| Sulu Sea | 143 | 231 |
| Celebes Sea | 140 | 155 |
| Eastern Equatorial Pacific | 100 | 114 |
| Northwest Australia | 53 | 60 |
| West Central Africa | 49 | 57 |
| Pacific Central America | 38 | 44 |
| Northwest South America | 24 | 40 |
| Total | 2011 | 3264 |

the complexity of multiple interacting factors. The propagation path of internal waves generally follows regions with significant changes in seafloor depth, especially near the continental shelf and islands. The propagation of internal waves exhibits periodicity and regularity, particularly under the modulation of tides (Li et al. (2024); Bai et al. (2023); Wang et al. (2013)). The SWOT satellite successfully captured internal wave signals over a large area in the South China Sea using high-resolution sea surface height data, particularly near deep-sea basins and straits between 15°N and 20°N, showcasing the advantages of SWOT in high-precision internal wave monitoring and revealing the spatial distribution characteristics of internal waves in this region.

The figure shows the distribution of internal wave detection in the Sulu Sea region using SWOT data. Compared to the South China Sea, internal wave signals in the Sulu Sea are mainly distributed between 7°N and 10°N. The internal wave observation points are relatively concentrated, particularly in areas with deeper seafloor depths. In the Sulu Sea, the generation of internal waves is closely related to the strong influence of tidal currents, particularly the semi-diurnal tide (M2) and diurnal tide (K1). These tidal currents interact with significant seafloor variations, such as the straits, reefs, and seafloor ridges of the Sulu Archipelago, to generate internal waves. As tidal currents pass through these regions, they trigger strong vertical density changes, resulting in internal wave formation. The propagation of internal waves in the Sulu Sea is influenced by background currents and seafloor topography. The propagation path typically follows the direction of the currents. Background flows induced by tidal currents significantly impact the speed and direction of internal wave propagation. In particular, cyclonic currents cause the internal wave propagation path to bend. For example, in the western Sulu Sea, internal waves propagating from the

https://doi.org/10.5194/essd-2025-822
Preprint. Discussion started: 25 February 2026




Pearl Bank region tend to bend westward, while internal waves originating from the Sibutu Passage propagate northeastward. The complex hydrological conditions and topographic features of the Sulu Sea provide favorable conditions for the generation and propagation of internal waves. The successful observation of these internal waves by SWOT data demonstrates its potential in middle and small-scale ocean processes(Huang et al. (2024, 2025); Rong et al. (2025)).

According to SWOT satellite data, the spatial distribution of internal waves in the Celebes Sea is mainly concentrated near the straits and areas connected to the Sulu Sea and Makassar Strait. Internal wave signals are particularly dense in these regions, reflecting the strong tidal effects and complex seafloor topography that influence internal wave generation in the area. In these regions, the generation and propagation of internal waves are jointly regulated by factors such as tidal currents, wind speed, and seafloor topography. The internal waves in the Celebes Sea are primarily triggered by tidal currents, particularly those from the Mindanao Current and Makassar Strait. When these tidal currents pass over seafloor ridges and canyons, the strong water flow disturbances generate internal waves. When tidal currents flow through irregular seafloor topography, density differences in the water column lead to the formation of internal waves, especially under the influence of semi-diurnal tides (M2), which significantly enhance internal wave generation. Since the Celebes Sea is connected to the Sulu Sea and Makassar Strait, the generation of internal waves is closely linked to the changes in water flow in these straits. The interaction between water flow and seafloor topography, particularly in these narrow regions, generates strong tidal disturbances, which, in turn, lead to internal wave formation. The propagation paths of internal waves in the Celebes Sea show typical periodic and directional characteristics. Internal waves mainly propagate along the straits and deep-sea basins, especially along the path from the Mindanao Passage to the Makassar Strait. Due to the influence of tidal currents and seafloor topography, internal waves undergo refraction or reflection during propagation, leading to changes in their propagation path. The propagation of internal waves is also influenced by background flows, and the wave speed and amplitude change as the internal waves encounter regions with varying depths(Hu et al. (2021); Chen et al. (2018)). The SWOT satellite provides high-precision capture of the spatiotemporal distribution of internal waves in the Celebes Sea, offering a profound understanding of the dynamic changes of internal waves.

The internal wave detection results from the SWOT satellite indicate that the distribution of internal waves in the Northwest Australia region is primarily concentrated on the continental shelf and areas connected to deep-sea basins, particularly near straits and seafloor ridges. As shown in the figure, most internal waves occur in the waters between 20°S and 15°S. This distribution pattern is closely related to the interaction between the region's seafloor topography and tidal currents. On the continental shelf and nearshore areas, where topographic variations are more pronounced, the frequency and intensity of internal wave generation are higher. In the Northwest Australia region, the generation mechanism of internal waves is mainly influenced by the combined effects of tidal currents and seafloor topography. Internal wave generation is primarily driven by tidal currents, especially those from the northern continental shelf and slope regions of Australia. When these tidal currents pass over uneven seafloor topography (such as straits and seafloor ridges), they induce strong vertical density changes, which trigger internal wave formation. When tidal currents pass over steeper seafloor regions, the amplitude and energy of internal waves significantly increase. The propagation of internal waves in the Northwest Australia region typically occurs along areas with significant changes in seafloor depth. After originating from the continental shelf or strait areas, internal waves propagate along regions with steeper seafloor gradients, particularly between seafloor ridges and deep-sea basins. The propagation

https://doi.org/10.5194/essd-2025-822
Preprint. Discussion started: 25 February 2026




path of internal waves is closely associated with the direction of tidal currents, usually exhibiting periodic and directional characteristics(Holloway and Serebryany (2023); Whitwell et al. (2024); Rayson et al. (2019)).

The internal wave detection results from the SWOT satellite in the Indonesia region show that the distribution of internal waves is widespread, covering nearly the entire Indonesian archipelago and surrounding seas. The internal wave signals are primarily concentrated between 0°N and 15°S, covering the waters around major islands such as Sumatra, Kalimantan, Java, and Sulawesi, especially in the straits, deep-sea basins, and continental shelf regions. The regions with the densest distribution of internal wave signals are the Sulawesi Sea, Sulu Sea, Makassar Strait, and Banda Sea. These areas experience a higher frequency of internal wave occurrence, particularly near complex seafloor topographies, such as the boundary between shallow seas and deep-sea basins, where internal wave generation and propagation are more pronounced. Spatially, internal waves in the Indonesia region primarily occur in deep-water areas, particularly along the continental shelf and seafloor ridges. In shallow seas, internal waves are less frequent, though distinct internal wave signals can also be observed in the transition zones between deep and shallow waters. The internal waves in the Indonesia region are primarily triggered by the interaction between tidal currents and seafloor topography. Specifically, in areas such as the Sulawesi Sea and Sulu Sea, tidal currents passing through straits, seafloor ridges, and shallow water areas cause strong internal tides due to density differences in the water, thereby generating internal waves. For example, the Sibutu Strait, a shallow water strait, is often a hotspot for internal wave formation. The propagation paths of internal waves in the Indonesia region typically follow the boundaries of straits and deep-sea basins. Especially from the Sulawesi Sea to the Sulu Sea, internal waves propagate along deep-water areas at the continental shelf edge, influenced by tidal currents and seafloor topography. Many internal waves are formed by the nonlinear intensification of internal tides. As tidal currents pass over seafloor undulations, vertical stratification and nonlinear effects in the flow increase, causing internal tides to evolve into internal waves. For example, when tidal currents pass through the Sibutu Strait in the Sulawesi Sea, the internal tide undergoes intense nonlinear changes, gradually transforming into large-amplitude internal waves. During the propagation of internal waves, the seafloor topography attenuates the wave energy. For instance, when internal waves encounter seafloor ridges, straits, or deep-sea basins, the wave intensity weakens and the waveform changes(Purwandana et al. (2023); As-Syakur et al. (2025); Purwandana et al. (2022)).

The red pentagram markers in the figure indicate the internal wave observation locations in the Eastern Equatorial Indian Ocean region using SWOT data. It can be seen that the internal wave signals are widely distributed in this area, primarily concentrated between 0° and 10°N in the equatorial region, covering waters between 86°E and 94°E. The detection density of internal waves is relatively high, especially in the deep-water areas of the eastern equatorial Indian Ocean and regions bordering deep-sea basins. From the figure, it is evident that internal wave signals exhibit higher density in certain specific areas, particularly around the Maldives and surrounding waters. The higher frequency of internal waves in this region indicates significant interactions between tidal currents and seafloor topography. The distribution of internal waves is also associated with straits, deep-sea basins, and continental shelf boundaries, which are typically hotspots for internal wave generation and propagation. The spatial distribution of internal waves is closely related to seafloor topography. Internal wave signals are particularly dense along the continental shelf edge, near straits and seafloor highs. In the eastern equatorial Indian Ocean, internal waves are primarily generated through the interaction of tidal currents with seafloor topography. In particular, at large

https://doi.org/10.5194/essd-2025-822
Preprint. Discussion started: 25 February 2026


seafloor features like the Mascarene Ridge, tidal currents passing through these areas create internal waves at the pycnocline (the water layer where density changes rapidly). The generation of these internal waves is closely related to the phase of the tidal currents, with larger amplitudes typically occurring in areas with significant tidal variations. Internal waves usually propagate along areas with significant changes in seafloor depth. In regions with complex seafloor topography, such as the Mascarene Ridge, internal waves can propagate over long distances, with energy gradually dissipating as they propagate. Studies show that internal waves originating from the Mascarene Ridge can propagate over thousands of kilometers, gradually losing energy and interacting with other wave patterns. As the internal waves propagate over long distances, their amplitude gradually decreases(Meng et al. (2022); Zhuang et al. (2022); Da Silva et al. (2015); Morozov et al. (1999)).

According to the SWOT internal wave detection distribution map for the Western Equatorial Atlantic, it can be observed that the spatial distribution of internal waves is primarily concentrated in the equatorial region between 3°N and 13°N, covering a vast area of water between 30°W and 50°W. The regions with dense internal wave occurrences are primarily located in deeper areas, especially at the boundaries of deep-sea basins, seafloor ridges, and continental shelves in the tropical Atlantic, where internal wave signals are more prominent. The distribution density of internal waves is particularly notable near the equator and in areas with significant changes in water depth. These regions typically exhibit strong tidal influences and complex seafloor topography, such as seafloor highs, deep-sea trenches, and straits, which play a crucial role in the generation and propagation of internal waves. The internal waves in the Western Equatorial Atlantic are mainly generated through the interaction between tidal currents and seafloor topography, especially at the seafloor highs and fault zones of the Mid-Atlantic Ridge (MAR). Internal waves are not confined to their generation regions but can propagate over large distances. Studies have shown that internal waves in the Western Equatorial Atlantic can propagate over large areas, reaching distances of several hundred kilometers, with their waveform gradually changing, though their energy diminishes during propagation. The SWOT internal wave detection distribution map for the West Central Africa region shows that the spatial distribution of internal waves is mainly concentrated between 5°N and 13°N, covering a wide area from 14°E to 29°W. Similar to the Western Equatorial Atlantic, the dense regions of internal wave signals are concentrated around deep-sea basins and seafloor ridges, particularly near the continental shelf and deep-water areas of West Central Africa, where the frequency of internal wave occurrence is higher. The generation mechanism of internal waves in the West Central Africa region is also associated with the interaction of tidal currents passing through deep-water areas, especially near deep-sea trenches and ridges. When strong tidal currents pass through these regions, internal tides are generated, and these internal tides form internal wave packets through nonlinear effects, propagating along areas with significant changes in water depth(Grigorenko et al. (2016); Vic and Ferron (2023); Santos-Ferreira et al. (2022); Da Silva et al. (2025)).

The SWOT internal wave detection distribution map for the Eastern Equatorial Pacific indicates a clear clustering pattern, with internal wave signals primarily concentrated around the equatorial region. These internal wave signals are widely distributed, covering a vast area from 87°W to 137°W, with particularly dense concentrations in regions with deeper seafloor depths and the presence of the thermocline. The distribution of internal waves is closely related to tidal currents and seafloor topography (such as straits and deep-sea basins). When tidal currents pass through these areas, they generate intense internal waves, especially at the intersection of the equatorial countercurrent and the eastward equatorial current. In the Eastern

https://doi.org/10.5194/essd-2025-822
Preprint. Discussion started: 25 February 2026




**Table 3.** Comparison of Multi-source Remote Sensing Data Availability in the Sulu Sea Region in 2024.

| | SWOT | Sentinel-1 C-SAR | Sentinel-3 OLCI |
|---|---|---|---|
| Number of data for the covered area in 2024 | 225 | 998 | 1165 |
| Number of data with detected internal waves in 2024 | 67 | 20 | 22 |
| Data availability rate | 29.78% | 2.01% | 1.89% |

Equatorial Pacific, internal wave generation is mainly caused by Tropical Instability Waves (TIWs). These waves are typically generated by shear in the equatorial currents, particularly in the strong shear zones between the equatorial undercurrent (EUC) and the North Equatorial Current (NEC). In this region, the interaction between tidal forces and the thermocline induces internal tides that excite internal waves. The generated internal waves usually appear as long wave packets with wavelengths reaching several hundred kilometers and exhibit strong nonlinear characteristics, allowing them to propagate over long distances in the ocean. In the Pacific Central America region, internal waves are distributed along the coastal deep-water areas and near the continental shelf. The distribution of internal waves in the Northwest South America region is mainly concentrated in areas connected to the Peru and Colombia straits, where seafloor topography and tidal currents play a significant role in internal wave generation and propagation. In the Northwest South America region, the internal wave generation mechanism is similar to that in the Eastern Equatorial Pacific, influenced primarily by equatorial currents and the thermocline. Tidal forces and seafloor topography in southwestern South America play a crucial role in internal wave formation, particularly near islands and seafloor highs, where internal wave generation is more frequent(da Silva et al.; Santos-Ferreira et al. (2023); Johnston and Colin (2022); van Haren et al. (2022)).

### 4.2 Statistical Analysis of Internal Wave Data in Different Sea Areas

This study constructed a global multi-region SWOT internal wave dataset based on 21,682 SWOT passes from 2023 to 2025. A total of 2,011 SWOT passes detected internal wave signals, identifying 3,264 internal waves. Table 2 presents the number of SWOT data and the detected internal waves in 13 high-frequency internal wave regions.

As shown in Table2, there is considerable variation in the amount of SWOT observational data for internal waves across different regions. The Indonesia region has the highest number of detection passes, reaching 280, followed by the South China Sea with 252 passes and the Eastern Equatorial Indian region with 238 passes. These regions exhibit higher internal wave observation densities, likely due to the frequent internal wave activity and long-term monitoring in these areas. In contrast, the Northwest South America region has only 24 passes, and the Pacific Central America region has only 38 passes, indicating relatively fewer internal wave observations. A comparison of the number of detected internal waves reveals that the Andaman Sea has the highest number, with 580 internal waves detected, suggesting very frequent internal wave activity in this region. This can be attributed to the complex seabed topography and strong tidal forces in the area, which promote frequent internal wave generation and propagation. The Indonesia region detected 476 internal waves, and the Eastern Equatorial Indian region detected 46 internal waves, reflecting higher internal wave counts and indicating active internal wave generation mechanisms. In

https://doi.org/10.5194/essd-2025-822
Preprint. Discussion started: 25 February 2026


Open Access Earth System Science Data Discussions

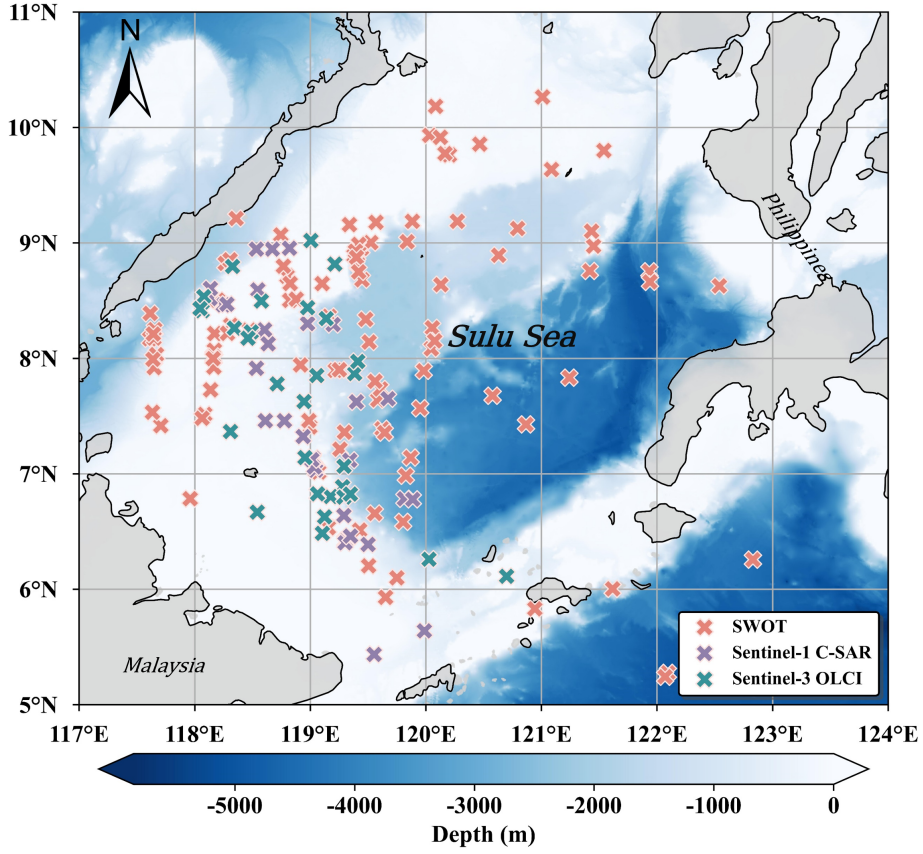


**Figure 9.** Spatial Distribution Map of Internal Wave Observations Using Multi-source Remote Sensing Data in the Sulu Sea Region in 2024.

contrast, the Northwest South America region detected only 40 internal waves, and the Pacific Central America region detected only 44, showing relatively low internal wave activity. The distribution of internal wave data and counts in the table indicates that regions with strong internal wave generation mechanisms typically have higher observational data and wave counts. For example, the Indonesia and South China Sea regions, influenced by strong tidal forces and complex seabed topography, exhibit frequent internal wave activity, with large amounts of SWOT data and a high number of detected internal waves. The internal wave generation mechanisms in these regions are primarily driven by tidal currents, thermocline interactions, and seabed topography, resulting in a high frequency of internal wave generation. In contrast, the Northwest South America and Pacific Central America regions exhibit lower internal wave counts, likely due to weaker internal wave generation mechanisms or reduced influence from tidal currents. However, as illustrated in the table, the rankings of internal wave data and counts do not always align. For instance, although the Andaman Sea does not have the highest data volume, it records the highest number of detected internal waves, further underscoring its characteristic role as a region with frequent internal wave activity.

https://doi.org/10.5194/essd-2025-822
Preprint. Discussion started: 25 February 2026




### 4.3 Comparative Analysis of SWOT and Other Data Sources

This study presents a detailed statistical analysis of three different remote sensing datasets for the Sulu Sea region in 2024, including SWOT altimetry data, Sentinel-1 C-SAR data, and Sentinel-3 OLCI optical data. Table3 summarizes the statistical results of these datasets in internal wave observation. The results show that Sentinel-3 OLCI optical data has the largest total number of images in the Sulu Sea, with 1,165 images, of which only 22 successfully detected internal wave signals. Sentinel-1 C-SAR data is slightly less, with a total of 998 images, of which 20 detected internal waves. SWOT data, with the smallest total number of 225 passes, successfully observed internal wave signals in 67 passes. This suggests that although the number of SWOT data is relatively smaller, its data availability for internal wave detection far exceeds that of SAR and optical data, highlighting the unique advantages of SWOT data in internal wave detection.

Figure9 illustrates the spatial distribution of internal wave observations in the Sulu Sea based on SWOT data, Sentinel-1 C-SAR data, and Sentinel-3 OLCI optical data. By analyzing the number of internal wave data from these three remote sensing sources and visualizing the internal wave observation results in the Sulu Sea region, it is evident that SWOT data outperforms Sentinel-1 C-SAR and Sentinel-3 OLCI data in terms of both observation count and spatial coverage. This is due to the all-weather observation capability of the SWOT satellite, which enables it to provide high-resolution sea surface height measurements, effectively covering larger areas and delivering consistent observational data. In contrast, although Sentinel-1 C-SAR also has all-weather observation capability, the sensor is not continuously active for persistent observation. Its limited observation range results in a more sparse spatial distribution of internal wave observations. While Sentinel-3 OLCI optical data provides a large spatial coverage, its observation quantity and quality are limited by weather factors such as clouds and fog. Overall, SWOT data demonstrates significant advantages in internal wave observation, particularly in terms of coverage and data continuity. It provides more precise and reliable support for the spatiotemporal analysis of internal waves, giving SWOT unique potential in multi-source remote sensing data fusion and internal wave detection.

### 4.4 Internal Wave Tracking Using Multi-Source Data

The statistical results from different data sources demonstrate that a single satellite remote sensing dataset is inadequate for monitoring the continuous variation of internal waves, which limits the ability to track internal waves using satellite remote sensing methods. However, the inclusion of SWOT data facilitates the integration of multi-source remote sensing datasets, enabling effective tracking of internal waves across the entire time series, thereby overcoming the limitations of relying on a single remote sensing data source. As shown in Figure10, on March 11, 2024, at 09:18:39, SWOT detected an internal wave signal. Figure10(a) presents the SWOT observation result, Figure10(b) shows the SAR image obtained by Sentinel-1 C-SAR on March 12, 2024, at 21:48:55, and Figure10(c) provides a combined display of both payload data types, with the red box highlighting the corresponding area where the internal wave occurred.

Figure11 presents a quantitative comparison along the profile for two typical internal wave observation locations. Figure11(a) shows the SSHA variation at the IW1 location from SWOT data, Figure11(b) shows the SSHA variation at the IW2 location from SWOT data, Figure11(c) displays the backscatter coefficient (Sigma0) variation at the IW1 location from Sentinel-1 C-

https://doi.org/10.5194/essd-2025-822
Preprint. Discussion started: 25 February 2026




SAR data, and Figure11(d) shows the Sigma0 variation at the IW2 location from Sentinel-1 C-SAR data. Figure11(d) shows that the SSHA profile from SWOT and the Sigma0 profile from C-SAR exhibit good consistency in terms of peak-to-trough location, phase, and amplitude variation trends. A comparison reveals that at the same location, approximately 36 hours apart, the internal wave streaks observed by SWOT and Sentinel-1 C-SAR are consistent in spatial position and morphology, almost perfectly overlapping in both location and shape. This indicates that after approximately three and a half tidal cycles, the internal wave reappears at the same location with nearly the same morphology, revealing its significant semi-diurnal tidal modulation characteristics and strong reproducibility. The synergistic observation between SWOT and Sentinel-1 C-SAR enables cross-platform data validation, providing strong support for the identification and study of internal wave periodic characteristics. This further validates the effectiveness of cross-platform validation and the feasibility of internal wave tracking using multi-source remote sensing data.

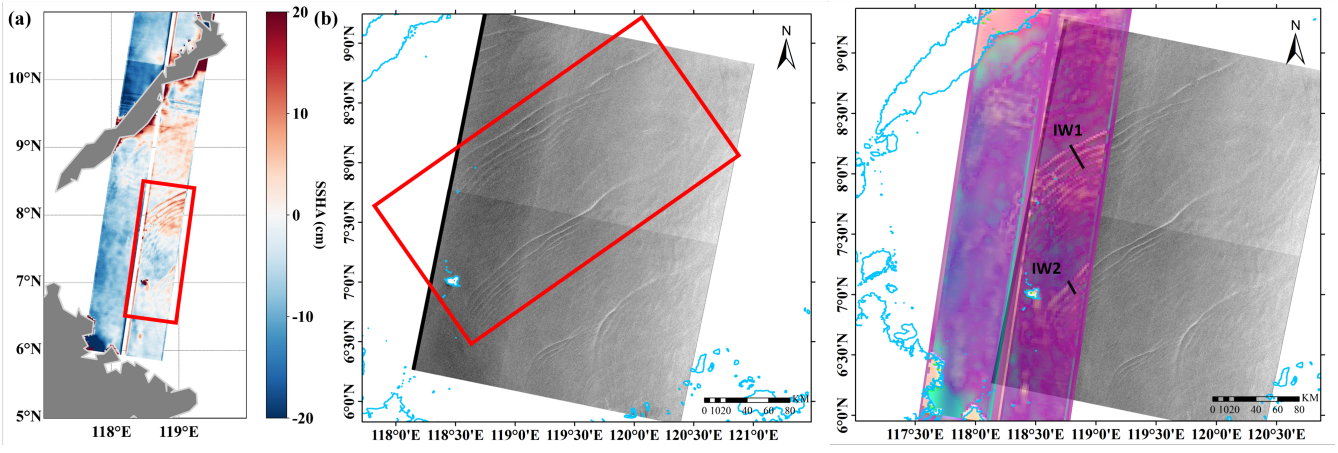


**Figure 10.** An example of an internal wave detected by SWOT on 11 March 2024, at 09:18:39 UTC. (a) corresponds to the SWOT data, (b) shows the SAR image (from Sentinel-1 C-SAR, acquired on 12 March 2024 at 21:48:55 UTC), and (c) presents an overlay display of the data from the two payloads. The red box indicates the corresponding area where the internal wave appears.

### 4.5 Unique Signals Observed by SWOT

Figure12 presents the internal wave observation results from SWOT data compared with Sentinel-3 OLCI optical data. Through comparative analysis, it is clear that the internal wave signal observed by SWOT on September 4, 2024, at 05:40 (shown in Figure12(a)) is highly consistent with the observation results from Sentinel-3 OLCI on September 4, 2024, at 02:15 (shown in Figure12(b)). It is worth noting that both datasets used a unified UTC time system, providing an accurate basis for the spatiotemporal comparison of the data. Although the internal wave signals exhibit a displacement between the two observations, their morphology remains largely unchanged, demonstrating the periodicity and stability of the internal wave signals. However, further image comparison reveals that SWOT successfully captured some internal wave signals that were not detected by Sentinel-3 OLCI. This discrepancy can be primarily attributed to cloud cover and the inherent limitations of optical sensors,

https://doi.org/10.5194/essd-2025-822
Preprint. Discussion started: 25 February 2026


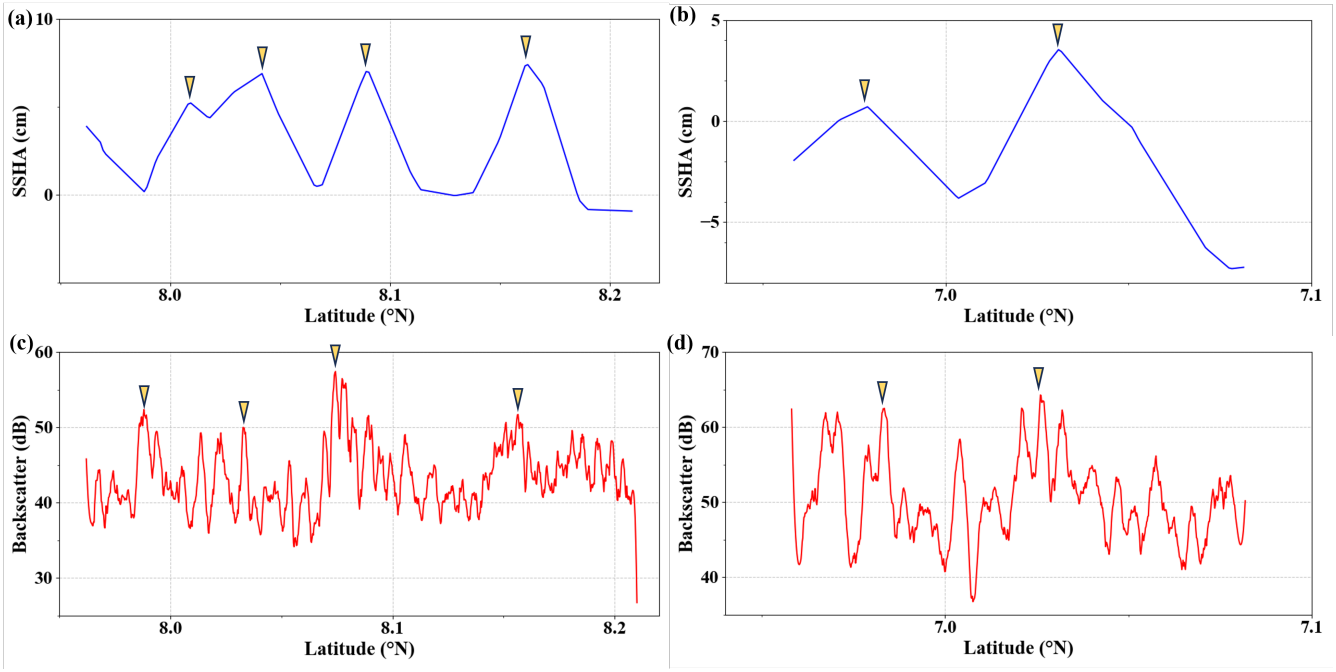


**Figure 11.** Data profiles for two internal wave observation locations. (a) SSHA variation at the IW1 location from SWOT data, (b) SSHA variation at the IW2 location from SWOT data, (c) Sigma0 variation at the IW1 location from Sentinel-1 C-SAR data, (d) Sigma0 variation at the IW2 location from Sentinel-1 C-SAR data.

which may prevent optical data from capturing clear signals in certain conditions. This finding further underscores the unique advantages of SWOT in internal wave observation, particularly in providing a more comprehensive and efficient observational perspective without the constraints of optical data.

Additionally, as shown in Figure13, SWOT observed a distinct internal wave signal on April 25, 2024, at 13:58:18 (Figure13(a)). Surprisingly, approximately 12 hours later, on April 26, 2024, at 02:11:29, a nearly identical internal wave signal was found in the Sentinel-3 OLCI optical data (Figure13(b)). Figure13(c) shows the overlay of the two images. The high temporal and spatial consistency observed indicates that the synergistic observation between SWOT and Sentinel-3 OLCI provides strong data support for the periodic detection of internal waves. This collaborative use of multi-source data not only helps validate the stability and consistency of internal wave signals but also enhances the accuracy of capturing internal wave characteristics. The SWOT data also revealed internal wave signals that were not captured by Sentinel-3 OLCI, particularly in areas affected by cloud cover or limited optical data resolution. This phenomenon further confirms the breakthrough advancement of SWOT as a next-generation imaging altimeter in internal wave detection.

The two specific observation examples above highlight the breakthroughs and the importance of the data support achieved by SWOT in internal wave observation. These unique findings not only demonstrate the advantages of SWOT in terms of observational accuracy, temporal resolution, and spatial coverage, but also provide unprecedented perspectives and data for

https://doi.org/10.5194/essd-2025-822
Preprint. Discussion started: 25 February 2026


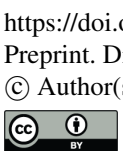



internal wave research. SWOT data provides a more comprehensive tool for internal wave monitoring, laying a solid foundation for future oceanographic research and environmental monitoring. Additionally, the high-precision imaging capability of SWOT and its advantage of being unaffected by weather conditions further enhance the scientific value and practical application prospects of internal wave observation.

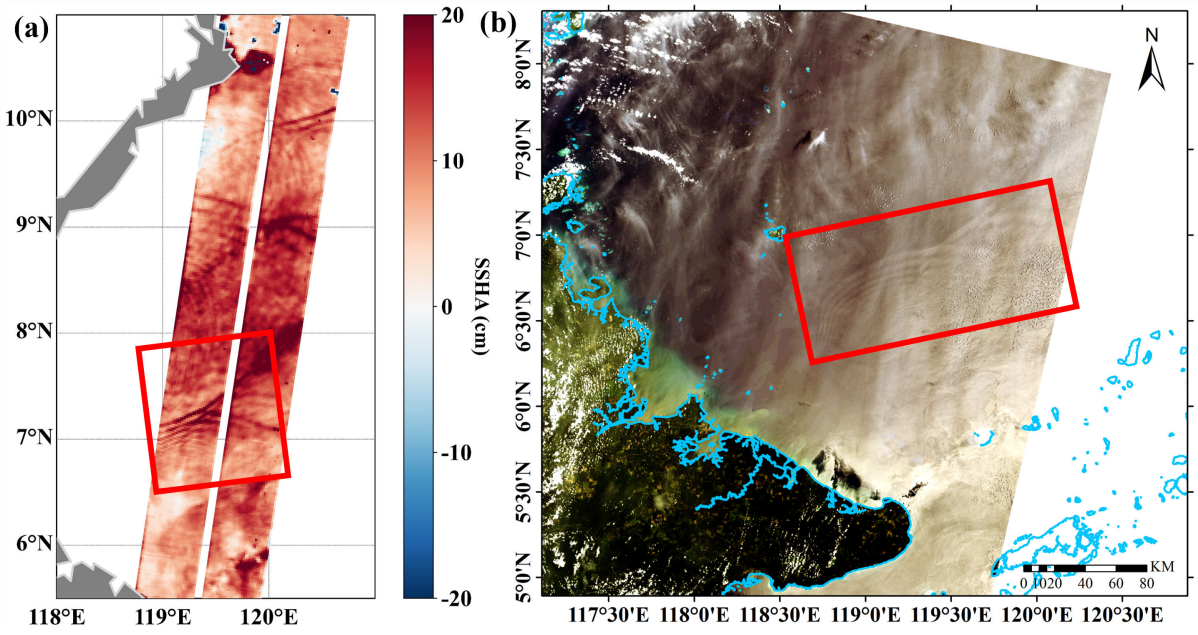


**Figure 12.** An example of an internal wave detected by SWOT on 04 September 2024 at 05:40 UTC. (a) corresponds to the SWOT data, (b) shows the optical image (from Sentinel-3 OLCI, acquired on 04 September 2024 at 02:15 UTC). The red box indicates the corresponding area where the internal wave appears.

## 5 Data availability

The internal wave dataset can be freely downloaded from https://doi.org/10.5281/zenodo.17666852 (Xi et al. (2025)).

All data used in this study are publicly accessible. The SWOT Level-3 KaRIn SSH data are available from the AVISO+ repository for ocean products: https://aviso-data-center.cnes.fr/user/ssalto/modules/3652 (AVISO/DUACS, 2024). Bathymetry data come from the GEBCO Compilation Group (2024) *GEBCO 2024 Grid* (https://doi.org/10.5285/1c44ce99-0a0d-5f4f-e063-7086abc0ea0f). Sentinel data were obtained from the Copernicus Marine Environment Monitoring Service (CMEMS): https://dataspace.copernicus.eu/.

https://doi.org/10.5194/essd-2025-822
Preprint. Discussion started: 25 February 2026


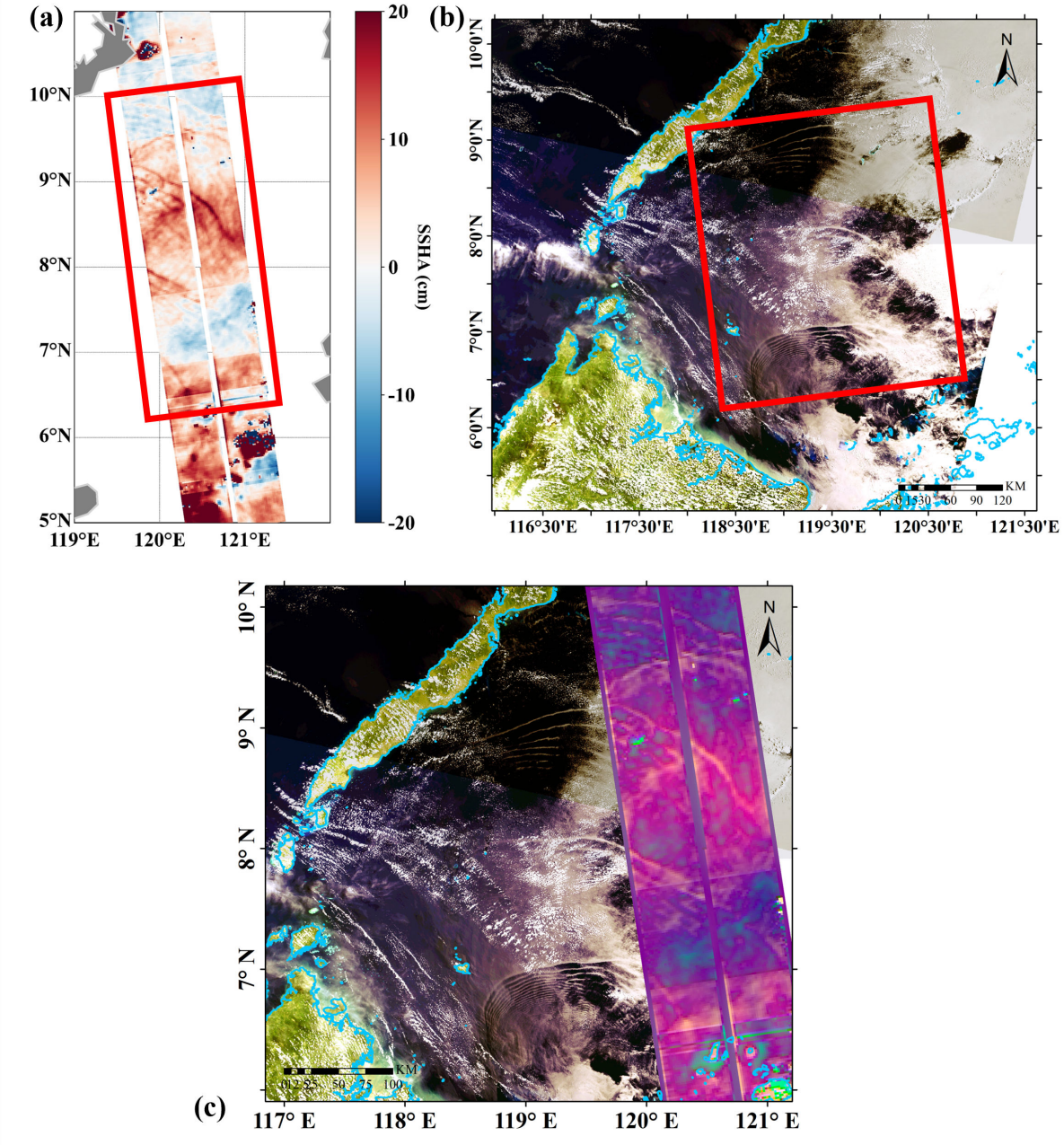


**Figure 13.** An example of an internal wave detected by SWOT on 25 April 2024 at 13:58:18 UTC. (a) corresponds to the SWOT data, (b) shows the optical image (from Sentinel-3 OLCI, acquired on 26 April 2024 at 02:11:29 UTC), and (c) presents an overlay display of the data from the two payloads. The red box indicates the corresponding area where the internal wave appears.

https://doi.org/10.5194/essd-2025-822
Preprint. Discussion started: 25 February 2026




## 6 Conclusions

This study employed SWOT data to conduct deep learning-based detection of internal waves across 13 global regions, successfully constructing an internal wave dataset using SWOT data from 2023 to 2025. The dataset includes not only the SWOT L2 data for each region but also the coordinates of the bounding boxes for the detected internal wave signals, along with the central latitude and longitude information for each detection location.

The results of this study demonstrate that the SWOT satellite is capable of effectively monitoring and capturing internal wave signals across major global oceanic regions, particularly in areas with strong tidal currents and complex seabed topography, such as the Andaman Sea, Indonesia, South China Sea, and Eastern Equatorial Indian Ocean. These regions exhibit a higher volume and frequency of internal wave observations due to the complexity of internal wave generation mechanisms and the strong interaction between tidal currents and seabed topography. Through comparisons of internal wave detection data and the number of internal waves, the study finds that the internal wave observation data volume and quantity in the Indonesia region are among the highest, indicating a high frequency of internal wave generation and significant influence from the interaction between tidal currents and seabed topography. In contrast, regions such as Northwest South America and Pacific Central America show relatively lower internal wave data volumes and quantities.

This study presents a thorough comparison and analysis of internal wave observations in the Sulu Sea region for 2024, utilizing three different data sources: SWOT altimetry data, Sentinel-1 C-SAR data, and Sentinel-3 OLCI optical data. The results highlight the significant advantages of SWOT in internal wave monitoring, with a data availability rate of 29.78%, far surpassing the data availability rates of 2.01% for Sentinel-1 C-SAR and 1.89% for Sentinel-3 OLCI optical data. The synergistic observation between SWOT and Sentinel-1 C-SAR demonstrates the consistency of internal wave signals in both time and space, validating the periodic characteristics of internal waves. These results further confirm the unique advantages of the SWOT satellite in internal wave monitoring, particularly in terms of coverage and data continuity, providing strong support for multi-source remote sensing data fusion and internal wave tracking. In the comparison between SWOT and Sentinel-3 OLCI optical data, it was found that SWOT can capture internal wave signals in certain regions that optical data cannot detect, especially in areas affected by cloud cover or limitations in optical sensor resolution. This highlights the significant potential of SWOT's high-resolution sea surface height measurements to overcome the constraints of optical data, offering a more comprehensive and efficient approach for internal wave monitoring. Overall, SWOT demonstrates unparalleled advantages in internal wave monitoring, particularly in terms of data volume, spatial coverage, temporal resolution, and accuracy, providing more precise and reliable support for spatiotemporal analysis of internal waves. The successful application of SWOT has not only enhanced the scientific value of internal wave monitoring but also laid a solid foundation for future oceanographic research, environmental monitoring, and early disaster warning.

In conclusion, the SWOT internal wave dataset constructed in this study provides crucial data support for internal wave research. It not only offers internal wave labels for artificial intelligence-based detection but also presents new perspectives for multi-source data research on internal waves. In future work, by integrating the SWOT dataset with multi-source remote sensing data and utilizing artificial intelligence techniques, the research can expand from two-dimensional sea surface height

https://doi.org/10.5194/essd-2025-822
Preprint. Discussion started: 25 February 2026




information to a three-dimensional understanding of internal wave structures. This will enable a more comprehensive and accurate understanding of the generation, propagation, and attenuation of internal waves. With this dataset, researchers can further investigate the relationship between internal waves and oceanic environments, climate change, ocean dynamics, and other factors, thereby advancing the application and development of ocean remote sensing technologies in internal wave monitoring. Moreover, the continuous updating and optimization of the SWOT internal wave dataset will provide additional data support and theoretical foundations for studies on internal wave monitoring and ocean mixing effects caused by internal waves.

*Author contributions.* X.X. and J.C. processed the data, drafted the manuscript, and revised and proofread it in English. G.C. and C.M. provided funding for the project. Y.G. and Y.L. conceived the idea and designed the experiments.

*Competing interests.* The contact author has declared that neither of the authors has any competing interests.

*Acknowledgements.* This work was supported in part by the National Natural Science Foundation of China under Grant 42276179, in part by Laoshan Laboratory Science and Technology Innovation Projects under Grant LSKJ202201302, and in part by Taishan Scholars Program tsqn202312281.

https://doi.org/10.5194/essd-2025-822
Preprint. Discussion started: 25 February 2026


Open Access Earth System Science Data Discussions

## References

Arvelyna, Y.: THE APPLICATION OF WAVELET ANALYSIS FOR INTERNAL WAVE DETECTION IN SAR AND OPTICAL IMAGES DATA OVER TSUSHIMA STRAIT, International Journal of Remote Sensing and Earth Sciences (IJReSES), 2, 2010.

As-Syakur, A. R., Raharja, I. M. D., Osawa, T., et al.: Estimation of Internal Solitary Waves Propagation Speeds and Occurrence using Long-term Sentinel-1 SAR Data in the Lombok Strait, Indonesia, IEEE Journal of Selected Topics in Applied Earth Observations and Remote Sensing, 2025.

Bai, X., Lamb, K. G., Liu, Z., and Hu, J.: Intermittent generation of internal solitary-like waves on the northern shelf of the South China Sea, Geophysical Research Letters, 50, e2022GL102 502, 2023.

Cai, T., Zhao, Z., D'Asaro, E., Wang, J., and Fu, L.-L.: Internal tide variability off Central California: multiple sources, seasonality, and eddying background, Journal of Geophysical Research: Oceans, 129, e2024JC020 892, 2024.

Cao, Z., Meng, J., Wang, J., Sun, L., and Zhang, H.: Study on the Forecasting of Internal Solitary Wave Propagation in the Andaman Sea Using Joint Ascending-Descending Orbit Sentinel-1A Data and Machine Learning, IEEE Journal of Selected Topics in Applied Earth Observations and Remote Sensing, 2024.

Chen, X., Qiu, B., Chen, S., Cheng, X., and Qi, Y.: Interannual modulations of the 50-day oscillations in the Celebes Sea: Dynamics and impact, Journal of Geophysical Research: Oceans, 123, 4666–4679, 2018.

Cui, G., Yuen, K.-V., Cai, Z., Liu, Z., and Zhang, G.: Research on adaptive ocean remote sensing target detection framework: An efficient solution based on the broad learning system, ISPRS Journal of Photogrammetry and Remote Sensing, 229, 188–210, 2025.

da Silva, J., Magalhaes, J. M. R., Santos-Ferreira, A. M., and Huerre, R.: Longevity of Internal Solitary Waves in the Pacific Cold Tongue: Synergies with Swot, Available at SSRN 5196730.

Da Silva, J., Buijsman, M., and Magalhaes, J.: Internal waves on the upstream side of a large sill of the Mascarene Ridge: A comprehensive view of their generation mechanisms and evolution, Deep Sea Research Part I: Oceanographic Research Papers, 99, 87–104, 2015.

Da Silva, J., Magalhães, J., Bosser, A., Huerre, R., Koch-Larrouy, A., Goret, C., Diallo, S., de Macedo, C. R., and da Silva, A. C.: Internal solitary wave parameters from SWOT KaRIn sea surface topography: A case study in the tropical Atlantic, Science of Remote Sensing, p. 100307, 2025.

Duo, Z., Wang, W., and Wang, H.: Oceanic mesoscale eddy detection method based on deep learning, Remote Sensing, 11, 1921, 2019.

Fu, L.-L., Pavelsky, T., Cretaux, J.-F., Morrow, R., Farrar, J. T., Vaze, P., Sengenes, P., Vinogradova-Shiffer, N., Sylvestre-Baron, A., Picot, N., et al.: The surface water and ocean topography mission: A breakthrough in radar remote sensing of the ocean and land surface water, Geophysical Research Letters, 51, e2023GL107 652, 2024.

Gan, X., Huang, W., Yang, J., and Fu, B.: Internal wave packet characterization from SAR images using empirical mode decomposition (EMD), in: 2008 Congress on Image and Signal Processing, vol. 4, pp. 750–753, IEEE, 2008.

Gan, X.-l., Huang, W.-g., Yang, J.-s., Zhou, C., and Shi, A.: A new method to extract internal wave parameters from SAR imagery with Hilbert-Huang transfrom, JOURNAL OF REMOTE SENSING-BEIJING-, 11, 39, 2007.

Garrett, C. and Munk, W.: Internal waves in the ocean, Annual review of fluid mechanics, 11, 339–369, 1979.

Geng, X., Li, T., Wu, X., and Yan, X.: Estimation of Internal Wave from Sentinel-1A Images by the Combination of 2-D and 1-D Empirical Mode Decomposition, in: Proceedings of EUSAR 2016: 11th European Conference on Synthetic Aperture Radar, pp. 1–4, VDE, 2016.

Grigorenko, K., Makarenko, N., Morozov, E., Tarakanov, R. Y., and Frey, D.: Stratified flows and internal waves in the Central West Atlantic, in: Journal of Physics: Conference Series, vol. 722, p. 012011, IOP Publishing, 2016.

https://doi.org/10.5194/essd-2025-822
Preprint. Discussion started: 25 February 2026




Holloway, P. and Serebryany, A.: A Variety of Transformations of Nonlinear Internal Tidal Waves of the Northwestern Shelf of Australia, in: Doklady Earth Sciences, vol. 509, pp. 153–159, Springer, 2023.

Hu, B., Meng, J., Sun, L., and Zhang, H.: A study on brightness reversal of internal waves in the Celebes Sea using Himawari-8 images, Remote Sensing, 13, 3831, 2021.

Huang, L., Yang, J., Ma, Z., Liu, B., Ren, L., Liu, A. K., and Chen, P.: Generation of diurnal internal solitary waves (ISW-D) in the Sulu Sea: From geostationary orbit satellites and numerical simulations, Progress in Oceanography, 225, 103 279, 2024.

Huang, L., Yang, J., Ren, L., Ma, Z., Chai, Y., Chen, P., He, S., Liu, B., and Liu, A. K.: Real and long-time predicting the trajectories of internal solitary waves: Case studies in the Sulu Sea, Ocean Engineering, 325, 120 765, 2025.

Jackson, C.: Internal wave detection using the moderate resolution imaging spectroradiometer (MODIS), Journal of Geophysical Research: Oceans, 112, 2007.

Johnston, T. S. and Colin, P. L.: Upwelling and downwelling driven by the North Equatorial Countercurrent and internal waves at Hatohobei Island and Helen Reef, Palau, Journal of Geophysical Research: Oceans, 127, e2021JC017 606, 2022.

Kang, J., Zhang, J., Song, P., and Meng, J.: The application of two-dimensional EMD to extracting internal waves in SAR images, in: 2008 International Conference on Computer Science and Software Engineering, vol. 1, pp. 953–956, IEEE, 2008.

Lee, Y.-H. and Kim, H.-J.: Comparative Analysis of YOLO Series (from V1 to V11) and Their Application in Computer Vision, Journal of the Semiconductor & Display Technology, 23, 190–198, 2024.

Li, X., Liu, B., Zheng, G., Ren, Y., Zhang, S., Liu, Y., Gao, L., Liu, Y., Zhang, B., and Wang, F.: Deep-learning-based information mining from ocean remote-sensing imagery, National Science Review, 7, 1584–1605, 2020.

Li, Z., Wang, J., Chen, X., Lu, K., Chang, Z., Lu, Y., and Wang, X.: Observation of Mode-2 Internal Solitary Waves in the Northern South China Sea Based on Optical Remote Sensing, IEEE Journal of Selected Topics in Applied Earth Observations and Remote Sensing, 17, 11 550–11 562, 2024.

Lien, R.-C., Tang, T., Chang, M., and d'Asaro, E.: Energy of nonlinear internal waves in the South China Sea, Geophysical Research Letters, 32, 2005.

Liu, A. K. and Hsu, M.: Internal wave study in the South China Sea using synthetic aperture radar (SAR), International Journal of Remote Sensing, 25, 1261–1264, 2004.

Liu, B. and D'Sa, E. J.: Oceanic internal waves in the Sulu–Celebes Sea under sunglint and moonglint, IEEE transactions on geoscience and remote sensing, 57, 6119–6129, 2019.

Liu, B., Yang, H., Zhao, Z., and Li, X.: Internal solitary wave propagation observed by tandem satellites, Geophysical Research Letters, 41, 2077–2085, 2014.

Ma, Y., Meng, J., Sun, L., and Ren, P.: Oceanic internal wave signature extraction in the Sulu Sea by a pixel attention U-Net: PAU-Net, IEEE Geoscience and Remote Sensing Letters, 20, 1–5, 2022.

Ma, Z., Huang, L., Yang, J., Ren, L., Li, X., He, S., Liu, B., and Liu, A. K.: Transformer-based hierarchical multiscale feature fusion internal wave detection and dataset, Ocean-Land-Atmosphere Research, 3, 0061, 2024.

Ma, Z., Zhou, L., Wu, D., and Zhang, X.: A small object detection method with context information for high altitude images, Pattern recognition letters, 188, 22–28, 2025.

Mandal, A. K., Seemanth, M., and Ratheesh, R.: Characterization of internal solitary waves in the Andaman Sea and Arabian Sea using EOS-04 and sentinel observations, International Journal of Remote Sensing, 45, 1201–1219, 2024.

https://doi.org/10.5194/essd-2025-822
Preprint. Discussion started: 25 February 2026




Meng, J., Sun, L., Zhang, H., Hu, B., Hou, F., and Bao, S.: Remote sensing survey and research on internal solitary waves in the South China Sea-Western Pacific-East Indian Ocean (SCS-WPAC-EIND), Acta Oceanologica Sinica, 41, 154–170, 2022.

Meng, J., Zhang, H., Sun, L., and Wang, J.: Remote sensing techniques for detecting internal solitary waves: a comprehensive review and prospects, IEEE Geoscience and Remote Sensing Magazine, 12, 46–78, 2024.

Morozov, E., Vlasenko, V., Demidova, T., and Ledenev, V.: Tidal internal wave propagation over large distances in the Indian Ocean, Oceanology, 39, 42–46, 1999.

Pan, Z., Zhai, Z., Li, Q., Li, Q., Wu, L., and Bao, L.: Preliminary Investigation of the Spatial-Temporal Characteristics and Vertical Dynamics of Internal Solitary Waves in the South China Sea from SWOT Data, Journal of Marine Science and Engineering, 13, 304, 2025.

Purwandana, A., Cuypers, Y., Bourgault, D., Bouruet-Aubertot, P., and Santoso, P. D.: Fate of internal solitary wave and enhanced mixing in Manado Bay, North Sulawesi, Indonesia, Continental Shelf Research, 245, 104 801, 2022.

Purwandana, A., Cuypers, Y., Surinati, D., Iskandar, M. R., and Bouruet-Aubertot, P.: Observed internal solitary waves in the northern Bali waters, Indonesia, Regional Studies in Marine Science, 57, 102 764, 2023.

Qiu, B., Chen, S., Wang, J., and Fu, L.-L.: Seasonal and fortnight variations in internal solitary waves in the Indonesian Seas from the SWOT measurements, Journal of Geophysical Research: Oceans, 129, e2024JC021 086, 2024.

Rayson, M. D., Jones, N. L., and Ivey, G. N.: Observations of large-amplitude mode-2 nonlinear internal waves on the Australian North West shelf, Journal of Physical Oceanography, 49, 309–328, 2019.

Rodenas, J. A. and Garello, R.: Wavelet analysis in SAR ocean image profiles for internal wave detection and wavelength estimation, IEEE Transactions on Geoscience and Remote Sensing, 35, 933–945, 1997.

Rong, Y., Yang, Y., Wang, C., Li, H., Li, J., and Huang, X.: Internal Tide Generation and Propagation in the Sulu Sea Under the Influence of Circulation, Journal of Marine Science and Engineering, 13, 806, 2025.

Santos-Ferreira, A., Silva, J. d., St-Denis, B., Bourgault, D., and Maas, L.: Internal solitary waves within the cold tongue of the equatorial pacific generated by buoyant gravity currents, Journal of Physical Oceanography, 53, 2419–2434, 2023.

Santos-Ferreira, A. M., da Silva, J. C., Magalhaes, J. M., Amraoui, S., Moreau, T., Maraldi, C., Boy, F., Picot, N., and Borde, F.: Effects of surface wave breaking caused by internal solitary waves in SAR altimeter: Sentinel-3 Copernicus products and advanced new products, Remote Sensing, 14, 587, 2022.

Simonin, D., Tatnall, A., and Robinson, I.: The automated detection and recognition of internal waves, International Journal of Remote Sensing, 30, 4581–4598, 2009.

Sun, L., Liu, Y., Meng, J., Fang, Y., Su, Q., Li, C., and Zhang, H.: Internal solitary waves in the central Andaman sea observed by combining mooring data and satellite remote sensing, Continental Shelf Research, 277, 105 249, 2024.

Svergun, E., Sofina, E., Zimin, A., and Kruglova, K.: Seasonal variability of characteristics of nonlinear internal waves in the Kuril-Kamchatka region by Sentinel 1 data, Continental Shelf Research, 259, 104 986, 2023.

van Haren, H., Voet, G., Alford, M. H., and Torres, D. J.: Internal wave breaking near the foot of a steep East-Pacific continental slope, Progress in Oceanography, 205, 102 817, 2022.

Vasavi, S., Divya, C., and Sarma, A. S.: Detection of solitary ocean internal waves from SAR images by using U-Net and KDV solver technique, Global Transitions Proceedings, 2, 145–151, 2021.

Vic, C. and Ferron, B.: Observed Structure of an Internal Tide Beam Over the Mid-Atlantic Ridge, Journal of Geophysical Research: Oceans, 128, e2022JC019 509, 2023.

https://doi.org/10.5194/essd-2025-822
Preprint. Discussion started: 25 February 2026




690 Wang, J., Huang, W., Yang, J., Zhang, H., and Zheng, G.: Study of the propagation direction of the internal waves in the South China Sea using satellite images, Acta Oceanologica Sinica, 32, 42–50, 2013.

Wang, X., Wang, J., Zhang, X., and Liu, J.: SWOT observation revealed internal solitary wave characteristic variations in the Lombok Strait, Journal of Oceanology and Limnology, pp. 1–14, 2025.

Whitwell, C., Jones, N., Ivey, G., Rosevear, M., and Rayson, M.: Ocean mixing in a shelf sea driven by energetic internal waves, Journal of
695 Geophysical Research: Oceans, 129, e2023JC019 704, 2024.

Xi, X., Chen, J., Chen, G., Li, Y., Ma, C., and Gai, Y.: SWOT Internal Wave Dataset, https://doi.org/10.5281/zenodo.17666852, zenodo, 2025.

Yang, Z., Lan, X., and Wang, H.: Comparative Analysis of YOLO Series Algorithms for UAV-Based Highway Distress Inspection: Performance and Application Insights, Sensors, 25, 1475, 2025.

700 Yu, Y., Xu, T., Wang, J., Wang, S., Li, Q., Meng, J., Chen, X., Lu, K., and Wang, G.: On the generation and evolution of internal solitary waves in the Andaman Sea, Journal of Ocean University of China, 22, 335–348, 2023.

Zhang, H., Fan, C., Sun, L., and Meng, J.: Study of the ability of SWOT to detect sea surface height changes caused by internal solitary waves, Acta Oceanologica Sinica, 43, 54–64, 2024.

Zhang, X. and Li, X.: Constructing a 22-year internal wave dataset for the northern South China Sea: spatiotemporal analysis using MODIS
705 imagery and deep learning, Earth System Science Data, 16, 5131–5144, 2024a.

Zhang, X. and Li, X.: Unveiling three-dimensional sea surface signatures caused by internal solitary waves: insights from the surface water ocean topography mission, Journal of Oceanology and Limnology, 42, 709–714, 2024b.

Zhuang, Z., Zheng, Q., Yang, Y., Song, Z., Yuan, Y., Zhou, C., Zhao, X., Zhang, T., and Xie, J.: Improved upper-ocean thermodynamical structure modeling with combined effects of surface waves and M 2 internal tides on vertical mixing: a case study for the Indian Ocean,
710 Geoscientific Model Development, 15, 7221–7241, 2022.